

SOLAR WIND **MAGNETIC** FIELDS

Edward J. Smith
Jet Propulsion Laboratory
California Institute of Technology
Pasadena, CA 91109-8099

ABSTRACT

The magnetic fields originate as coronal fields that are convected into space by the supersonic, infinitely conducting, solar wind. On average, the sun's rotation causes the field to wind up and form an Archimedes Spiral. However, the field direction changes almost continuously on a variety of scales and the irregular nature of these changes is often interpreted as evidence that the solar wind flow is turbulent. To a surprising extent, the large-scale field near the ecliptic (solar equator), where observations have been made (between 0.3 and 35 AU), appears to be dominated by dipole-like fields from the sun's polar corona. The (open) field lines, however, are attached to the sun at only one end, the other end being carried off into the outer heliosphere by the solar wind. The oppositely-directed fields in the northern and southern hemispheres are separated by a thin, wavy current sheet that encloses the sun and extends throughout the heliosphere. A complication to this otherwise straight-forward description is the presence of solar wind structure associated with high speed streams that corotate with the Sun. Another cause of structure is the (frequent) presence of Coronal Mass Ejections whose origins, magnetic topology, internal dynamics and interaction with the pre-existing solar wind are still being actively studied. Recent interest has also been directed to understanding the topology of the field between the shock that is thought to terminate the supersonic solar wind flow and the heliopause. The three-dimensional field properties at high latitudes and in the vicinity of the polar heliosphere have attracted recent interest as a result of the Ulysses mission. A brief description of the recent results obtained when this spacecraft reached the Sun's south pole are included.

Introduction

The **heliospheric** magnetic field (**HMF**) was called the interplanetary magnetic field (**IMF**) for many years until observations became available beyond the outermost planets of the solar system and significantly far above and below their orbit planes. Our understanding of the large scale field and the processes which shape it are ultimately derived from Parker's solar wind model. The model provides the baseline against which all the observations have been compared and has been modified as necessary to accommodate departures from the simple set of assumptions that underlie it.

In presenting his model, **Parker** anticipated significant departures of the solar wind from simple radial solar wind flow at constant speed. Thus, solar activity was expected to generate shock waves that would propagate rapidly outward through the pre-existing solar wind. At great distances, the solar wind was anticipated to interact with the magnetized interstellar plasma, forcing it out of the solar system and thereby creating the **heliosphere**. A termination shock was visualized inside the **heliosphere** at which the supersonic solar flow **would** become subsonic before it reaches the boundary of the **heliosphere** called the **heliopause**. The above **are** only a few examples of the large scale solar wind structure which have been the object of study ever since the first extensive space measurements became available.

This review addresses both the average properties and the many forms of large scale structure in the solar wind magnetic field. Properties of this pervasive, magnetic field based on observation and theory will be described from its origin in the solar corona all the way to the **heliopause** as well as from the equator to the pole.

The Spiral Angle

The basic elements of the solar wind **field** in the solar equator are shown in Figure 1 (Parker, 1963). The field lines are seen to **all** originate at the sun as coronal fields that are carried off by the radially-flowing supersonic solar wind represented by **the** radial arrows. The most basic property of the fields is the spiral form which results from their connection at one end to the rotating Sun. The analogy is often made to a rotating lawn sprinkler where the water droplets although moving radially outward lie on a spiraled locus. Alternatively, one can imagine the solar wind plasma to be sliding along a rotating field line while simultaneously moving radially outward (consider the pickup arm of a phonograph). The dashed circle represents the distance to the Earth's orbit (1 astronomical unit, AU).

The original Parker figure has been modified to include information regarding the field polarity. Arrows have been added to distinguish outward (positive) fields from sunward (negative) fields. In addition, appropriate pluses and minuses have been added just inside the circle to denote polarity. This representation explains the origin of the term, magnetic sector, to describe the polarity. The circle is thereby divided into pie-shaped sectors (two sectors as shown here but occasionally the circle is divided into four or even six sectors).

The expression for the spiral angle, ψ , in the usual spherical coordinates (r, θ, ϕ) with the Sun's rotation axis as the pole, is:

$$\tan \psi = -r \frac{d\phi}{dr} = B_{\phi}/B_r = -\Omega r \sin \theta / V_r \quad (1)$$

Parker assumed a steady state with a radial solar wind velocity, V_r , independent of r . The **angular** rotation rate of the Sun is $\Omega = 2\pi/T$, where T is usually assumed to be the sidereal equatorial period of 25.4 days. A typical value for V_r is 420 km/s so that, at the orbit of Earth, $\psi = 45^\circ$ (rather than 55° as shown in Figure 1).

Given B_r and V_r , B_ϕ will automatically adjust to yield the spiral angle, equation (1). The sign of B_ϕ depends on the sign of B_r . It might be supposed that a B_θ component would be possible and it is commonly stated that Parker simply assumed it was zero. However, both the spiral angle and $B_\theta = 0$ are a consequence of the electric field vanishing in the solar wind frame (along with the assumptions of a steady state and $\vec{V} = V_r, 0, 0$). If an electric field was present in the infinitely-conducting, **collisionless** plasma infinitely large currents would develop. The mathematical details involving the electric and magnetic fields and currents associated with Parker's model have been relegated to an appendix.

Confirmation that the field lies in the $r\phi$ plane is presented in Figure 2. This histogram was obtained from Pioneer 10 and 11 measurements of the field latitude angle, δ_B , over the radial range from 1 to 8.5AU (Thomas and Smith, 1980). A very large number of hourly averages (43,484) are involved. The **north-south** component shows considerable variability with a width at half maximum of $\pm 30^\circ$. Nevertheless, the statistically significant average of δ_B is zero.

A histogram of the observed longitude angle of the field, ϕ_B , is shown in Figure 3. The hourly averages *represented here* come from the same data set as in Figure 2. In order to accommodate the changing spiral angle with distance, the measured fields were transformed into coordinates with one axis along the Parker Spiral assuming $\psi = 45^\circ$ at 1 AU ($\tan\psi = r$). Two peaks are seen corresponding to outward (0") and inward (180") spiral fields. The two peaks agree with the Parker Spiral angle with a high level of certainty.

Significant variability in the spiral angle is evident in Figures 2 and 3. What are the causes?

Differentiation of the basic equation for the spiral angle leads to

$$\delta(\tan \psi) = \frac{\Omega r}{V_r} \sin \theta \frac{\delta V_r}{V_r} - \frac{\sin \theta}{V_r} (\delta \Omega). \quad (2)$$

Two causes are seen: variations in the radial solar wind speed and departures of the magnetic field from strict coronation at the solar wind source. The latter are called stochastic variations by

Jokipii and Parker (1970) because they are expected to accompany irregular motions (random walk) of the field lines in the **photosphere** and **chromosphere**.

The relative effectiveness of these two **sources** of variability can easily be estimated numerically. What solar wind speeds would cause $\delta(\tan\psi) = +0.5$ or ψ to vary between 27° and 56° ? The low and high value of V_r are 260 and 700 km/s, rather extreme values observationally. This calculation shows that it is difficult to attribute the large variations observed over time scales of minutes to hours to variations in the solar wind **speed**.

The second term in equation (2) implies that, for the same variation, $\delta\Omega = (0.5) V_r/r$. At the Sun, (one solar radius, r_s), the equivalent transverse velocity would be $\delta V = r_s \delta\Omega = (0.5) V_r r_s/r \cong 1$ **km/sec**. Thus, modest motions on the Sun, perhaps associated with super granules, can cause large deviations in the field direction.

Another major source of variability of the spiral angle is the presence of waves or turbulence. The **Alfven** relation between the perturbations in the velocity and magnetic field associated with the waves is $\delta\vec{V} / \delta\vec{B} = C_A / B$, where C_A is the **Alfven speed**. **Observationally**, short period (≤ 3 hour) *fluctuations in the field* can cause deflections in direction of $\pm 45^\circ$ corresponding to $\delta B/B \approx 1$. It then follows that $\delta V \approx C_A$, typically 60 km/s at 1AU. Thus, relatively small transverse velocity variations, **approximately** equal to $V_r/10$, are associated with large angular field deflections.

The fact that $\delta V/C_A \approx 1$ is noteworthy since a ratio of the velocity perturbations to the wave speed of approximately one is generally taken to be a condition of strong turbulence. Since the solar wind is highly supersonic, it has often been **supposed** that the flow is turbulent and the language of turbulence carried over from fluid dynamics has often been applied in studies of the ever-present field fluctuations.

Sector Structure

That the sector structure is a large scale, persistent feature of the **heliospheric** field is borne out by Figure 4 (Smith et al., 1986). This figure represents a standard display of the sectors with each horizontal line, consisting of pluses, minuses and gaps (for missing data or indeterminate polarity), equivalent to a solar rotation of 27 days. The solar rotations are identified by their **Bartels** Rotation number, designated BR , running between numbers 1910 to 2039. Eight years of data, a major fraction of a solar cycle, are shown extending from 1974 to 1982. The right **half-**figure contains the polarities observed by Pioneer 11 as it traveled outward from 1.0 to beyond 10AU. Since the heliographic latitude of the spacecraft is changing throughout this interval, the latitudes **are** listed in the extreme right hand column. The corresponding sector structure at 1AU as observed by the two spacecraft, **ISEE-3** and IMP-8, is shown in the left half-figure for comparison. The general correspondence in the polarities between 1 AU and the outer **heliosphere** is evident.

An alternate representation of the stability of the sector **structure** is that in Figure 5, another histogram of the field longitude angle. The data shown are from more recent observations by Pioneer **11** in 1991 while the spacecraft was located at 35 AU. The striking feature of this histogram is the narrowness of the two peaks corresponding to the inward ($\approx 90^\circ$) and outward ($\approx 270^\circ$) Parker spiral. The Solar **Heliospheric (SH)** Coordinate System in which the angles are measured has the \mathbf{x} (or R) axis radially outward from the Sun, the z (or N) axis is northward in the plane of \mathbf{x} and the sun's rotation axis, H , while they (or T) axis completes the orthogonal set. Spacecraft typically do not lie in the solar equatorial plane so that R is not perpendicular to H . The field vector in curvilinear coordinates in this and the coordinate system introduced in the discussion of the **spiral** angle are simply related: $B_R = B_r, B_T = B_\phi, B_N = -B_\theta$.

Commonly-occurring tracking gaps in these kinds of data often make the assignment of daily polarities a hazardous undertaking because of the large implicit uncertainties. This **representation**, however, shows the extent to which the observations agree with the spiral angle and reveal the extent to which the field coincides with one of the polarities. There has been considerable speculation that the oppositely-directed fields would reconnect across the current sheet and that this would disrupt the sector structure at large distances. In spite of such prognostications, there is little, if any, evidence of a “filling-in” of the region between the two dominant polarities such as might be anticipated **if** reconnection was on-going.

The Solar Origin of the Magnetic **Field**

Many of the observed properties are consistent with the **field** originating at high solar latitudes. A commonly-held view of the relation between solar and solar wind magnetic fields is shown schematically in Figure 6. This sketch is a qualitative three-dimensional representation of the field topology derived rigorously by **Pneuman** and Kopp (1971). Basically, the “open” fields with one end at high latitude and the other end carried off by the solar wind, overlie “closed” **transequatorial** field lines which have both ends rooted in the Sun.

The open field lines can be identified with dark coronal holes. The closed fields contain trapped electrons which scatter visible radiation from the **photosphere** and are generally seen in **coronagraph** images in which they have the appearance of a bright arcade. The field lines at the top of the loop-like lower-lying fields tend to **form** a cusp or “streamer” so that the entire structure, which typically extends around the sun in the form of a thick disc, is called the coronal streamer belt (**CSB**).

It is seen that the **heliospheric** current sheet (the dotted **surface**) maps back to the sun along the streamer belt (**Hundhausen**, 1977; Smith et al., 1978; **Borini** et al., 1982). The figure shows that

the symmetry axis of the **HCS/CSB**, represented **here** by the equivalent magnetic axis, **M** , does not generally coincide with **the** sun's rotation axis. This tilt angle causes the current sheet to develop the form of a wavy ballerina skirt or hat brim as the sun rotates. Various representations of this wavy current sheet on a variety of **heliospheric scales** and for various tilt angles have appeared in the literature (e.g., see **Jokipii** and Thomas, 1981).

There are several **reasons** why knowledge of the current sheet location is important to studies of the solar wind. Although deformed, the HCS serves as the magnetic equator of the **heliosphere** and organizes many properties of the **heliospheric** particles. Figure 7 (**Zhao** and Hundhausen, 1981) shows the average dependence of the solar wind proton density and speed on the latitude above and below the current sheet (called **heliomagnetic** latitude). The density tends to be a maximum and the speed a minimum in the vicinity of the current sheet, general characteristics which have been widely observed in a large number of other studies.

The HCS has also been found to influence the intensities of high energy galactic cosmic rays (**GCR**) (**Jokipii** et al., 1977) and the anomalous cosmic ray (**ACR**) component (Lockwood et al., 1988) (which originates inside the **heliosphere** as a consequence of the pick-up of freshly-ionized interstellar neutrals followed by acceleration to high energies ≥ 10 MeV). The identification of fast or slow solar wind as originating in the northern or southern solar hemisphere can also be established by their location relative to the current **sheet**.

Detailed comparisons of the HCS with actual solar magnetic fields are possible by extrapolation of observed **photospheric** fields to a "solar wind **source surface**" (**Hoeksema** et al., 1983). **Line-of-sight** magnetic fields **derived** from synoptic observations by ground-based **magnetographs** are extrapolated upward from the photosphere into a spherical shell using a potential field model. In addition to the fields being prescribed at the inner boundary, the fields at the outer spherical

boundary, the source surface, are required to be radial and the resulting solution is computed as a sum of spherical harmonics.

On the source surface, there is a wavy neutral line along which $B = B_r = 0$ that separates oppositely-directed large scale fields. This neutral line is identified with the **heliospheric** current sheet. Figure 8 provides an example derived in October, 1991 (Hoeksema, 1992). The upper half figure contains the stronger, smaller scale **photospheric** fields while the lower half figure shows the weaker, larger scale fields after extrapolation into the “corona”. The **low** order, dipole term is clearly dominant at **the** source surface.

Application of this procedure to many successive solar rotations has revealed how the solar field changes with the solar cycle.’ Figure 9 shows the secular variation in the dipole term between 1976 and 1991, i.e., over the most recent sunspot cycle. The upper panel contains the north polar field strength which shows a maximum of ≈ 1 Gauss ($10^{-4}T$) near solar minimum (1976), vanishes at solar maximum (1979-1980) and then reverses polarity. The **field** strength increases to -2 Gauss at the succeeding minimum and the field is seen again to reverse polarity in **mid-1990**.

In addition to these changes with field strength or moment, the **dipole** changes orientation in a systematic fashion as shown in the middle panel. The latitude **angle** of the dipole is $\approx \pm 90^\circ$ near solar minimum (i.e., aligned with the sun’s rotation axis) and decreases to $\approx 0^\circ$ when the field reverses sign. The bottom **panel** addresses the inclination of the source surface neutral sheet (derived from its maximum variation in latitude during a **given** solar rotation). This parameter is closely related to the dipole “tilt” angle and is consistent with a low inclination of the neutral sheet at minimum and a high inclination at maximum.

The effect of the changing current sheet inclination and the reversal in polarity can both be observed in the sector structure. Figure 10, which is in basically the same format as Figure 4, shows observations during two successive solar minima in 1976 and 1986 (Smith, 1989). The polarities were observed by Pioneer 11 between 1 and 20AU at the north heliographic latitudes indicated in the columns denoted "LAT". Note the disappearance of the typical two sectors in the bottom half of both panels with the field pointing continuously outward in 1976 and inward in 1986. The obvious interpretation is that the current sheet inclination has decreased in both instances to less than $\sim 15^\circ$ so that the spacecraft is continuously above the current sheet and records only a single polarity.

A third disappearance of the sector structure at the approach to solar minimum has been observed recently by the Ulysses spacecraft at 30°S latitude (Smith et al., 1993). Thus, by virtue of having spacecraft positioned above or below the solar equator, the low inclination has been seen in three successive solar cycles.

The reversal in the sun's polarity was first observed by Rosenberg and Coleman (1969) using spacecraft data and subsequently by Svalgaard and Wilcox (1974) who based their analyses on interplanetary field polarities inferred from ground-based magnetic observations at high latitude. Both studies exploited the annual excursion of the Earth in heliographic latitude of $\pm 7\frac{1}{4}^\circ$ which leads to a yearly variation in $P(+)$, the relative fraction of the time a positive polarity is observed during each solar rotation.

Figure 11 contains the results of a similar type of analysis but one which is capable of higher time resolution. The solid curve is the difference in $P(+)$ at two spacecraft, Pioneer 11 which was enroute to 12AU and ISEE-3 which was stationed in a halo orbit about the first Sun-Earth libration point, L_1 , just inside 1AU. The dashed curve is the difference in the instantaneous latitudes, δ , of the two spacecraft. The principal features of note are the overall correlation

between the differences in P and δ and the 180° change in phase that occurred in 1979-1980 just at the time that the sun's polar caps reversed polarity.

Solar Wind Structure: Effect on the HMF

The solar wind exhibits considerable structure which is visible each solar rotation. It is caused by the wind originating **from** specific solar regions, such as coronal holes, and by the rotation of the Sun which allows fast wind to overtake and interact with slow wind from a **different** longitude.

The characteristic "stream-stream" interaction is shown schematically in Figure 12 (Belcher and Davis, 1971). The upper half-figure characterizes the interaction in terms of (solid) streamlines emanating from four **corotating** solar sources which lead to a slow-fast-slow-fast configuration. The streamlines are spiraled because the coordinate system is **corotating** with the sun. A spacecraft will appear to proceed along the circular arc in a clockwise sense. The dotted curves are lines of force of the solar wind magnetic field. The bottom half-figure shows the characteristic variation observed in the solar wind speed, V_w , and density, N , the field strength, B , the thermal speed (equivalent to **temperature**), V_T , the standard deviation in the magnetic field fluctuations, σ_S , and the azimuthal velocity component, V_ϕ .

The essential physics of the interaction leads to the development of compression regions (**Corotating Interaction Regions or CIRs**) alternating with rarefaction regions. The compression region consists of slow wind (**S**) that has been accelerated (**S'**) and fast wind (**F**) that has been decelerated (**F'**) separated by an interface at which the total solar wind internal pressure ($NkT + B^2/8\pi$) reaches a peak. The pressure gradient supplies the forces which alternately speed-up and slow-down the solar wind and cause the interaction region to widen continuously with distance.

The intersection of the magnetic field lines with the streamlines correspond to their crossing through a **collisionless** shock into the **CIR**. A forward shock (propagating outward from the Sun) develops along the leading edge of **the CIR** and a reverse shock (propagating sunward but convected outward by the **more rapidly**-moving supersonic solar wind) forms at the trailing edge. The consequences of the forward-reverse shock pair for the magnetic **field** and solar wind speed profiles are shown in Figure 13 (Smith and Wolfe, 1977). The upper two panels contain measurements over several days made at 4.3AU by Pioneer 10. The middle panel and the schematic below it show that the gradual increase in speed typical of observations at 1 AU has been replaced by two steps at the shocks.

The solar wind structure associated with the alternating compression and rarefaction regions becomes even more striking with increasing distance. As the interaction regions widen, they eventually begin to encounter one another and merge into even wider regions. Beyond 5- 10AU, a single large **CIR** is customarily observed each solar rotation. Evidently, the fastest-moving structure per rotation has overtaken and compressed the slower-moving structure ahead of it.

A good example of merging and its effect on solar wind structure can be seen in Figure 14 (Smith, 1985). The field magnitudes are shown at two different locations in 1984, at 16AU by Pioneer 11 and as measured at 1AU by **ISEE-3** (**lower** panel). At Pioneer, the field is seen to increase and decrease by a factor < 5 at periodic intervals **corresponding** to a solar rotation. The lower figure shows many more smaller increases associated with the passage by the spacecraft of several streams and **CIRs** each rotation.

The merging process is a dominant feature of the outer **heliosphere** and continues to operate to distances 250AU. By the time the solar wind reaches such distances, the successive **CIRs** evident in Figure 14 have also merged so that the solar wind structure over a year is typically dominated by a few very large Merged Interaction Regions (**MIRs**) in which enhancements in the

field, density and temperature extend over several solar rotations (e.g., McDonald and Burlaga, this conference and references therein). During solar maximum, this merging is especially effective when it is driven by very energetic Coronal Mass Ejections (CMEs) associated with major outbursts of solar activity (e.g., in March-June 1991).

Variations in Field Magnitude with Time and Distance

The magnetic field magnitude varies with the solar cycle in a systematic manner. In Figure 15 (Winterhalter et al., 1990), annual variations of B at 1AU are shown by the open squares (ISEE-3) and circles (omnibus values assembled by the National Space Science Data Center/NSSDC). The field has minima near solar minimum in 1976 and 1986-87. The field maxima occur near or just following solar maximum (1982, 1990).

It is interesting that B is largest near the time that the Sun's polar cap fields reverse (rather than becoming small or vanishing). The magnetic fields equivalent to the highly inclined HCS or to the magnetic axis having been rotated through $\approx 90^\circ$ now presumably originate in the Sun's equatorial regions.

The filled dots in Figure 5 represent measurements obtained by Pioneer 11 in the outer heliosphere (at the distances indicated along the top) which have been extrapolated back to 1AU using Parker's solar wind model and assuming $\psi = \pi/4$ at 1 AU (i.e., without correcting for variations in solar wind speed). Although the extrapolated field reproduces the solar cycle variation observed at 1 AU, there is a systematic difference with B being lower than expected at large distances.

This difference has been described as a magnetic "flux deficit". The solar magnetic flux is given by $\Phi = \int B_r dA$. Since $B_r \propto r^{-2}$, Φ becomes negligibly small compared to $B \approx B_\phi$ at large r and is difficult to determine in the presence of ever-present large transverse fluctuations. However,

equation (1) implies $\Phi = \int (VrB_\phi/\Omega) d\theta d\phi = \int VrB_\phi d\theta dt$ since $d\phi = \Omega dt$. Thus, the time average of $rB_\phi \approx B$ at large r is also a measure of Φ . In the Parker Model, Φ is constant and VrB_ϕ is an invariant.

The flux deficit seen in the Pioneer data has not been confirmed by Voyager observations over the same range of radial distances (Burlaga and Ness, 1993). Various possibilities have been proposed to explain the discrepancy, in particular, the relatively “high latitude” of Pioneer 11 and the influence of changes in V_r on the extrapolated field magnitude. However, the latitude of Pioneer has varied significantly between -5 and 15° over the life of the mission and the inclusion of the measured speed at Pioneer in the extrapolation has failed to account for the flux deficit (Winterhalter et al., 1990). At present, the reason for the deficit appearing in the Pioneer data but not in the Voyager data is unknown.

Apart from the observations, theories have been developed that anticipate a departure from the Parker model. The original suggestion was that the enhanced spiraling of the field near the solar equator leads to increased pressure there which then deflects the solar wind and magnetic field slightly poleward (Suess and Nemey 1975, Suess et al., 1985). In a more recent model, the tilted magnetic dipole and the characteristic heliomagnetic latitude dependence of the solar wind speed give rise to excessive equatorial pressure associated with stream-stream interactions (Pizzo and Goldstein, 1987). Either model can account for a deficit of the magnitude observed by Pioneer. This issue and its successful resolution in terms of the physical processes involved are not only of heliospheric interest, Astrophysicists have found processes such as that proposed by Suess and Nerney of interest in accounting for the formation and poleward displacement of jets.

Coronal Mass Ejections

Thus far, the discussion of solar wind structure has concentrated on the effect of fast and slow streams. Not all of the solar wind, however, issues **more** or less steadily from stable sources such as coronal holes. The issue of corotating versus transient sources of solar plasma has a long history. Before direct solar wind observations became available, a major point of controversy was the open spiraled field topology characteristic of Parker's model in contrast to magnetic "tongues" or "bottles", a model advocated by Gold (1962). In retrospect, as often happens, both models were valid.

The Parker model was confirmed first beginning in 1962 (Snyder and Neugebauer, 1964; Neugebauer and Snyder, 1966). Another 10 years passed before coronal mass ejections were conclusively identified, first in Skylab white light coronagraph images (e.g., see Zirker, 1977) and subsequently by **HELIOS** and other spacecraft. Therein lies a tale; it is difficult to distinguish the two types of **solar** wind on the basis of in-situ observations.

Although, as **Hundhausen** (this conference) has shown, CMES make a contribution to the total solar wind mass of only 1 to 10%, they exert a profound influence on solar wind structure on a global scale. The reason is **related** to the enormous expansion which CMES undergo as they travel outward into the **heliosphere**. Near the Sun, as the coronagraph images show, their characteristic scale is a solar radius or diameter. **However**, by the time they reach **1 AU**, they have grown to scales that are a significant fraction of an astronomical unit, often 0.1 to 0.2AU in radius with a comparable transverse dimension.

Two complementary reasons for this expansion have been suggested. A speed gradient between the leading and trailing edges of 50-100 **km/s** could be responsible. Alternatively, the expansion could be driven by excess internal pressure rather than by a free expansion.

The expansion is presumably responsible in part for the difficulty in identifying CME plasma and fields by direct observation. Another factor is the nature of the interaction between the CME and the preceding solar wind which bears a resemblance to fast-slow stream interactions. CMES are typically accompanied by a forward shock, a region of high pressure and irregular fields and, occasionally, by a reverse shock. Identification depends on a number of features being present more or less simultaneously such as lower than usual proton temperatures and densities, stronger and quieter than usual field strengths, the enhancement of helium relative to hydrogen, the presence of hi-directional electron and/or ion streams, etc.

A subset of CMES that have a distinctive magnetic topology which assists identification are so-called magnetic “clouds” (Burlaga, 1991). An example is shown in Figure 16 based on HELIOS data. Notable features, used to define clouds, are the enhanced field strength and a characteristic north-south field deflection which, in combination with the x component, indicates a large scale rotation of the field. The variations in the basic solar wind parameters are also fairly typical, namely, a decreasing speed from front to back, and regions of low density and temperature.

A schematic representation of two CME field topologies is presented in Figure 17 (Gosling, 1990). The upper figure represents magnetic loops (tongues or bottles) drawn out from the Sun by the plasma. The lower figure represents the fields as helical, a configuration that is often thought to be associated with force-free fields ($\vec{j} \times \vec{B} = 0$ implying a balance between magnetic pressure and magnetic tension forces). A number of comparisons between observed fields inside magnetic clouds and best fit force-free fields based, for example, on models such as those of Burlaga (1988), have yielded a close correspondence. However, as a final warning on the difficulty of generalizing the properties of CMEs, it has been estimated that *only 10% or less* of CMES fit the definition of magnetic clouds (Gosling, 1990),

Figure 17 actually presupposes (solely for convenience) the answer to a long-standing question: Do both ends of magnetic field lines inside the **CME** remain attached to the Sun or do they close on themselves to form detached loops? This global question has been difficult to answer with available in-situ measurements. Perhaps, both configurations occur at various times.

Near solar maximum, the Sun produces numerous very energetic **CMEs**, which lead to a restructuring of the global properties of the **heliosphere**. Active regions have the capacity to generate several ejections during a solar rotation which then propagate into the outer **heliosphere** over a range of longitudes. They can compress the slower-moving solar wind which preceded them to form global or large scale Merged Interaction Regions (**MIRs**) that occupy a large solid angle about the sun.

A kinematic simulation of this process is shown in Figure 18 (**Akasofu and Hakamada, 1983**). A series of six **CMES** are shown after they have left the sun and traveled into the outer **heliosphere**. This “snapshot” shows the formation of several merged regions represented by compressions of the magnetic field (the dark densely-packed azimuthal field lines) which alternate with very large rarefaction regions (the light nearly radial field lines). The contrast with spiral structures of the kind represented in Figure 12 is evident,

The Magnetic Field Near the **Heliopause**

Although the **Pioneers** and **Voyagers** have penetrated deeply into the outer **heliosphere**, they are still apparently a long distance from the bounding surface (the **heliopause**) between the solar and interstellar media. The scale of the **heliosphere** is uncertain at present but indirect evidence suggests a distance to the nose (closest approach) of ≈ 100 AU.

Before reaching the **heliopause**, the spacecraft are expected to pass through an inner shock at which the supersonic flow of the solar wind terminates, changes abruptly to a subsonic flow (hence, a termination shock) and is deflected away from **or** along the outer boundary to flow into the **heliotail** (Parker, 1963; Ax ford, 1972; Holzer, 1989). The crossing of the termination shock is being awaited anxiously (**Pesses** et al., 1993) and when observed should establish more definitively the distance to the **heliopause**. The shocked **solar** wind lies in the region between the termination shock and the **heliopause** called the **heliosheath**.

There is considerable research interest in several related questions. What is the nature of the shock? In particular, will its structure be modified fundamentally by energetic particles (anomalous cosmic rays which **are** thought to be accelerated at the shock and whose energy density may equal or exceed the solar wind energy density)? What is the character of the flow in the **heliosheath** (compressive or **non-compressive**)? Is merging or reconnection of the **heliospheric** and interstellar magnetic fields important?

The character of the magnetic field in the sheath and the influence of sector structure on magnetic merging are topics which have attracted attention recently. **The** results of a recent model **are** shown in Figure 19 based on potential flow (**Nerney** et al., 1993). The sphere at the center of the figure represents the inner termination shock, Streamlines of the flow are shown which appear to emanate from the sub-stagnation point to form a cylinder whose axis lies in the direction of the approaching interstellar wind. Field lines are shown along the side of the cylinder and are parallel to the flow in the plane corresponding to the solar equator and transverse to the flow in the plane containing the Sun's pole or rotation axis. The shaded sector coincides with three magnetic sectors whose polarities alternate as shown by the arrow heads.

Important features of the model are(1) the origin of the **field** lines lying on or near the **heliopause**, which all originate from or near the stagnation region, (2) a strong asymmetry in the

field orientation and strength between the equator and the pole, with the field being significantly stronger in the polar region, and (3) the varying polarity, which could imply a sequence of regions or "**stripes**" in which magnetic merging may take place. It will be interesting to determine ultimately to what extent provocative modes such as this are comet.

The 3D Magnetic Field: Recent Ulysses Results

Thus far, the discussion has emphasized the region of the **heliosphere** which we know best, namely, the fan-shaped region near the ecliptic plane in which all previous measurements have been made. The Parker model is basically three dimensional and the field topology is specified at all latitudes. Figure 20 shows three open field lines, one originating at the equator, the second at mid-latitude and the third in the polar region. The field lines are basically **helices** lying on the surfaces of cones whose axes are the Sun's rotation axis and with half-angles equal to the **co-latitude**, θ . As the figure shows, the fields are strongly spiraled near the equator, having the appearance of a coiled spring, and nearly radial in the polar regions.

A comparison of measured fields at **ISEE-3** and Pioneer Venus Orbiter over several years has exposed a latitude dependence in which the field strength is asymmetric about the equator (**Luhmann et al., 1988**). The field is weaker in the north in some years and stronger in the north in others. A comparison of Voyager 1,2 data at significantly different latitudes (-30°) also showed years in which the source field extrapolated back to 1 AU was either stronger or weaker at high latitude (**Burlaga and Ness, 1993**).

There are reasons to expect deviations from a simple dependence of B on $\sin \theta$, since the **photospheric/coronal** field is **inhomogeneous** and the solar wind speed and angular **rotation** rate of the Sun vary with latitude. Much new information, a testing of our current ideas and some unexpected surprises are eagerly anticipated as a result of the Ulysses mission.

The Ulysses mission profile appears in Figure 21 (Smith et al., 1991; Wenzel et al., 1992). It shows that the spacecraft was launched in October, 1990, traveled outward to Jupiter, arriving in February 1992, and used Jupiter's gravity to rotate the inclination of the elliptical orbit to traverse the Sun's south **polar** region in 1994.

After leaving the equatorial plane in 1992, Ulysses observations of the solar wind and magnetic field came to be dominated by a series of large corotating high speed streams with peak speeds ≥ 700 km/s (Phillips et al., 1994). The presence of these streams was a temporal effect, rather than a latitude dependence, similar streams being observed simultaneously by spacecraft in or near the ecliptic. When Ulysses reached -30° in May 1993, the sector structure disappeared showing that the spacecraft had risen above the maximum latitudinal extent of the **heliospheric** current sheet (Smith et al., 1993). Above this latitude, only **inward-directed** fields corresponding to the magnetic polarity of the Sun's south pole were seen.

Above $\approx -50^\circ$, the large streams and other solar wind structure essentially disappeared and Ulysses was continuously immersed in solar wind from the south polar coronal hole with a steady speed of ≈ 750 km/s (Phillips et al., 1995). On a few occasions, the tops of a **CME** were detected. The magnetic field was found to be highly variable in direction with $\Delta B/B \approx 1$ (Smith et al., 1995). Correlation of the field changes with simultaneous changes in the velocity demonstrated that the variations were caused by outward-propagating **Alfvén** waves having large amplitudes and periods extending up to tens of hours.

One of the most striking results involved the latitude gradient in the **radial** field component which is most easily related to the solar magnetic field. Many scientists, including those responsible for the source surface models described above, expected the field strength to increase with latitude owing to the influence of the Sun's magnetic dipole (Wang, 1995; Zhao and

Hoeksema, 1995). However, the measurements revealed the absence of a gradient with B_r being essentially uniform and independent of latitude (Balogh et al., 1995). Figure 22 shows $B_r r^2$ at Ulysses, averaged over successive latitude intervals of 5° , as a function of time and latitude. Measurements are also shown that were obtained simultaneously in the ecliptic by the spacecraft, IMP-8. The two data sets fail to show a significant difference as Ulysses traveled from the equator to the pole.

This result has important implications. Since the global photospheric field is much stronger in the polar caps, the absence of a gradient in the solar wind implies that magnetic flux is being transported equatorward. There must be a corresponding divergence of the solar wind flow from the polar coronal hole. The likely explanation is that the magnetic field is exerting a stress in the solar wind acceleration region that causes this divergence. The stronger polar cap fields near the Sun represent a gradient in magnetic pressure ($B^2/8\pi$) tending to push the plasma to lower latitudes. The observed uniformity of B_r at larger distances would be the end-result of these stresses having finally relaxed to a stable configuration. Models of coronal magnetic fields which include such stresses and the resulting solar wind divergence (Pneuman and Kopp, 1971; Suess et al., 1977) are confirmed by these Ulysses observations.

The spiral angle has also been studied as a function of latitude. The average angle has been computed from the averages of the components (indicated by brackets): $\langle \phi \rangle = \tan^{-1}(\langle B_\theta \rangle / \langle B_r \rangle)$. It has been compared with the Parker spiral angle, $\phi_p = \tan^{-1}(\Omega r \cos \delta / V_r)$, resulting in the histogram of the difference shown in Figure 23 which includes observations above 60° . The average differs from zero with $\langle \phi \rangle - \phi_p > 0$ which, for inward-directed fields, implies a departure toward a more radial direction (describable as an “underwinding” of the Parker spiral). This result agrees qualitatively with similar analyses carried out near the ecliptic using multi-spacecraft measurements.

However, the observed distribution function shows a large **departure** from a normal or Gaussian distribution. A marked asymmetry is present which favors large values of $\Phi_B - \Phi_P$ and which causes a significant difference between the average and most probable value. Up to $\approx -50^\circ$, the latter agreed with Φ_P , but at higher latitudes neither measure agrees with the Parker model. Presumably, Φ_B is being strongly affected by the large amplitude **Alfvén** waves and, until their effect is eliminated somehow, it is difficult to demonstrate the extent of the agreement with the model or to use the spiral angle to infer the solar rotation rate at high latitude.

Appendix

The spiral angle originates from basic physical considerations. An electric field, E , in inertial space will transform into the frame of reference moving with the solar wind as $E_w = E + \vec{V} \times \vec{B}$, where \vec{V} is the solar wind velocity and \vec{B} is the magnetic field. Since the solar wind is basically a **collisionless** plasma with **infinite** electrical conductivity, $E = J/\sigma$ must vanish for finite currents, J , implying $E = -\vec{V} \times \vec{B}$. Alternatively, the latter condition can be described conceptually by saying the magnetic field is frozen-into and moves with the plasma so that there is no relative motion to **generate** an E_w .

The E field in inertial space is the result of the Sun's B field rotating past the point of observation and is given by $\vec{E} = E_e = -\Omega r \sin \theta \vec{B}_r$, where Ω is the angular velocity of the Sun (or, more strictly, of the end of the field line) and θ is the **colatitude** in the usual spherical coordinates. For the case of a radial velocity, i.e., $\vec{V} = V_r$, $\vec{V} \times \vec{B} = V_r \vec{B}_\phi$. Hence, $E_e = -\Omega r \sin \theta \vec{B}_r - V_r \vec{B}_\phi$ or

$$B_\phi/B_r = \tan \psi = -\Omega r \sin \theta / V_r. \quad (1)$$

According to this equation, given V_r and B_r (a property of the solar field and generated by currents at the sun), B_ϕ will adjust to yield the appropriate spiral angle.

It might be supposed that a \mathbf{B}_θ component would be possible but it is excluded from Parker's model. It is all too often claimed that Parker simply assumed $\mathbf{B}_\theta = 0$ and that misunderstanding has led to confusion. For that reason, a derivation of $\mathbf{B}_\theta = 0$ *now* follows.

The general conditions are that $\mathbf{V} = V_r$ and $\frac{\partial}{\partial \phi} = \frac{\partial}{\partial t} = \frac{d}{dt} = 0$. The latter implies

$\partial \vec{\mathbf{B}} / \partial t + \mathbf{V} \cdot (\mathbf{V}_r \vec{\mathbf{B}}) = 0$ or $\mathbf{V} \cdot (\mathbf{V}_r \vec{\mathbf{B}}) = 0$. If a \mathbf{B}_θ component was present, the explicit expression becomes $\partial(r^2 \mathbf{V}_r \mathbf{B}_\theta) / \partial r = 0$. From $(\mathbf{V} \times \vec{\mathbf{E}})_\theta = -\partial \mathbf{B}_\theta / \partial t = 0$, it follows that

$\partial(r \mathbf{E}_\phi) / \partial r = \partial(\mathbf{V}_r \mathbf{B}_\theta) / \partial r = 0$. Since $\partial(r^2 \mathbf{V}_r \mathbf{B}_\theta) / \partial r = r^2 \partial(\mathbf{V}_r \mathbf{B}_\theta) / \partial r + 2r \mathbf{V}_r \mathbf{B}_\theta = 0$, $\mathbf{V}_r \mathbf{B}_\theta = 0$.

Finally, with $V_r \neq 0$, $\mathbf{B}_\theta = 0$.

An alternative derivation is to consider the electric field that would be associated with \mathbf{B}_θ , i.e., $\mathbf{E}_\phi = -\mathbf{V}_r \mathbf{B}_\theta$. Then, the voltage along a circle about the Sun would be $V = \oint \mathbf{E}_\phi \cdot d\mathbf{s} = -2\pi \mathbf{V}_r \mathbf{B}_\theta$.

However, $V = -\frac{d\Phi}{dt} = 0$, so that $\mathbf{B}_\theta = 0$.

The model also prescribes the currents that are responsible for \mathbf{B}_ϕ . The current associated with \mathbf{B}_ϕ can be computed from $\mathbf{V} \times \vec{\mathbf{B}} = \mu_o \vec{\mathbf{J}}$ and, as expected, is transverse to \mathbf{B}_ϕ , i.e.,

$j_r = -2(B_{r0} r_o) \sin \delta / \mu_o r^2$ where the radial field component is B_{r0} at $r_o = 1 \text{ AU}$ and δ is heliographic latitude. Thus, for an outward field in the northern hemisphere (be), the radial current is

inward, is zero on the equator and maximum at the pole. Since the Sun cannot be realistically represented as a magnetic **monopole**, a more physical model would have inward radial fields in the southern hemisphere. Since both B_{r0} and δ are negative, the associated radial currents are also inward. The inward currents north and south are compensated by an outward surface current at the equator such that the total current is zero as required (Smith et al., 1978). The

electromagnetic boundary condition applied at the equatorial interface between the two oppositely-directed fields leads to a linear surface current density, $\vec{\mathbf{K}}$:

$$K_r = 2B_{r0} r_o / \mu_o r, K_\phi = 2B_{r0} r_o^2 / \mu_o r^2$$

(conservation of magnetic flux requires that $B_r = B_{r0} r_0^2 / r^2$).

It can readily be shown that the net **current** out of the Sun is

$$I_r = 2 \int_0^{\pi/2} \int_0^{2\pi} j_r \cos \delta r^2 d\phi d\delta - \int_0^{2\pi} K_r r d\phi = 0$$

It is also seen that the field lines form Archimedes spirals (as is well known), since

$$-rd\phi/dr = B_\theta / B_r = -\Omega r \sin \theta / V_r, \text{ or } r = (V_r / \Omega \sin \theta) \phi.$$

The current streamlines on the equator form hyperbolic or reciprocal spirals. As above,

$$rd\phi/dr = K_\phi / K_r = r_0 / r, \text{ so that } \phi = \phi_0 + 1 - r_0 / r.$$

Acknowledgment

Portions of this manuscript present work done at the Jet Propulsion Laboratory of the California Institute of Technology for the National Aeronautics and Space Administration. The summary of recent Ulysses **results** was not possible at the time of the conference and was not presented there. However, it was added at the request of one of the referees to update the review with more recent information.

REFERENCES

- Akasofu, S.-I., and Hakamada, K. 1983. Solar wind disturbances in the outer **heliosphere**, caused by six successive solar flares from the same active region. *Geophys. Res. Lett.*, 10:577.
- Axford, W.I. 1972. The interaction of the solar wind with the interstellar medium. *Solar Wind*, NASA SP 308:609.

- Balogh, A., Smith, E. J., Tsurutani, B.T., Southwood, D. J., Forsyth, R. J., and Horbury, T.S. to appear 1995. Structure and Characteristics of the **Heliospheric** Magnetic Field over the South Polar Region of the Sun. *Science*.
- Belcher, J.W., and Davis, Jr., L. 1971. Large-amplitude **Alfvén** Waves in the Interplanetary Medium, 2. *J. Geophys. Res.*, **76**:3534.
- Borini, G., Gosling, J. T., Bame, S. J., and Feldman, W. C. 1982. Helium abundance enhancements in the solar wind. *J. Geophys. Res.*, **87**:7370.
- Burlaga, L. F. 1988. Magnetic clouds and **force-free** fields with constant alpha. *J. Geophys. Res.*, **93**:7217.
- Burlaga, L. F.. 1991. Magnetic clouds. In *Physics of the Inner Heliosphere II*, eds. R. Schwenn, and E. Marsch (New York: Springer-Verlag) pp. 1-22,
- Burlaga, L. F. and Ness, N. F. 1993. Radial and latitudinal variations of the magnetic field strength in the outer **heliosphere**. *J. Geophys. Res.*, **98**:3539.
- Gold, T. 1962. Magnetic storms. *Space Sci. Rev.*, **1**:100.
- Gosling, J.T., 1990. Coronal mass ejections and magnetic flux ropes in interplanetary space. In *Physics of Magnetic Flux Ropes*, eds. C. T. Russell, E. R. Priest and L. C. Lee (Washington, DC: Geophys. Monogr. Ser., 58, AGU) pp. 343-364.
- Hoeksema, J. T. 1992. Large scale structure of the **heliospheric** magnetic field: 1976-1991. In *Solar Wind Seven*, eds. E. Marsch and R. Schwenn (New York: Pergamon Press) pp. 191-196.
- Hoeksma, J. T., Wilcox, J. M. and Scherrer, P. H. 1983. The structure of the **heliospheric** current sheet: 1978-1982. *J. Geophys. Res.*, **88**:9910.

- Holzer, T.E.** 1989. Interaction between the solar wind and the interstellar medium. *Arm. Rev. Astron. Astrophys.*, 27:199-234.
- Hundhausen, **A.J.** 1977. An interplanetary view of coronal holes. In *Coronal Holes and High-Speed Wind Streams*, ed. **J.B. Zirker**, (Boulder: Colorado Associated University Press), p. 225.
- Jokipii, J. R., and Thomas, **B.T.** 1981. Effects of drifts on the transport of cosmic rays, IV, Modulation by a wavy interplanetary current sheet. *Astrophys. J.*, 243:1115.
- Jokipii, J. R.**, and Parker, E. N. 1970. On the convection, diffusion and adiabatic deceleration of cosmic rays in the solar wind. *Astrophys. J.*, 160:73.
- Jokipii, J. R., Levy, E. H., and Hubbard, W. B. 1977. Effects of particle drift on cosmic ray transport, I, General properties, application to solar modulation, *Astrophys. J.*, 213:861.
- Lockwood, **J. A.**, **Webber, W. R.**, and Hoeksema, J. T. 1988. Interplanetary cosmic ray latitudinal gradient in 1984 to 1987 using IMP8 and Voyager data. *J. Geophys. Res.*, 93:7521-7526.
- Luhmann, J. G., Russell, C. T., and Smith, E.J. 1988. Asymmetries of the Interplanetary Field Inferred from Observations. In *Proceedings of Sixth International Solar Wind Conference*, ed. V.J. Pizzo (NCAR Tech. Note 306) pp. 323.
- Nerney, S., **Suess, S. T.**, and **Schmahl, E. J.** 1993. Flow downstream of the heliospheric termination shock, *J. Geophys. Res.*, 98:15,169.
- Neugebauer, M. and Snyder, C. W. 1966. Mariner 2 observations of the solar wind, 1, average properties. *J. Geophys. Res.*, 71 :4469-4484.
- Parker, E. N. 1963. *Interplanetary Dynamical Processes*, Wiley -Interscience (New York).

- Pesses, M. E., Jones, W. V., and Forman, M. 1993. Voyager and Pioneer missions to the boundaries of the heliosphere. *J. Geophys. Res.*, **98**:15,123.
- Phillips, J. L., Balogh, A., Bame, S. J., Goldstein, B. E., Gosling, J. T., Hoeksema, J. T., McComas, D. J., Neugebauer, N., Sheeley, Jr., N. R., and Wang, Y.-M. 1994. Ulysses at 50° South: Constant Immersion in the High Speed Solar Wind. *Geophys. Res. Lett.*, **21**:1105-1108.
- Phillips, J. L., Bame, S. J., Feldman, W. C., Goldstein, B. E., Gosling, J. T., Hammond, C. M., McComas, D. J., Neugebauer, M., Scime, E. E., and Suess, S. T. to appear 1995. Ulysses Solar Wind Plasma Observations at High Southerly Latitudes. *Science*.
- Pizzo, V. J., and Goldstein, B. E. 1987. Meridional Transport of Magnetic Flux in the Solar Wind Between 1 and 10 AU: A Theoretical Analysis. *J. Geophys. Res.*, **92**:7241.
- Pneuman, G.W. and Kopp, R.A. 1971. Gas-magnetic field interactions in the solar corona. *Solar Phys.* **18**:258-270.
- Rosenberg, R. L. and Coleman, Jr., P. J. 1969. Heliographic latitude dependence of the dominant polarity of the interplanetary magnetic field, *J. Geophys. Res.*, **74**:5611.
- Smith, E. J., Page, D. E., and Wenzel, K.-P. 1991. Ulysses: A journey above the Sun's poles. *Eos Transactions*, **72**:241.
- Smith, E. J., Neugebauer, M., Balogh, A., Bame, S. J., Erdős, G., Forsyth, R. J., Goldstein, B. E., Phillips, J. L., and Tsurutani, B. T. 1993. Disappearance of the heliospheric sector structure at Ulysses. *Geophys. Res. Lett.*, **20**:2327-2330.
- Smith, E. J., Tsurutani, B. T., and Rosenberg, R. L. 1978. Observations of the interplanetary sector structure to heliographic latitudes of 16°: Pioneer 11. *J. Geophys. Res.* **83**:717.

- Smith, E. J., **Slavin**, J. A., and Thomas, B. T. 1986. The **heliospheric** current sheet: 3 dimensional structure and solar cycle changes. In *Proceedings of the ESLAB Symposium on the Three Dimensional Structure of the Heliosphere* (Hingham, Mass.: D. Reidel Pub. Co.) p. 267.
- Smith, E. J., and Wolfe, **J.H.** 1977. Pioneer 10, 11 Observations of Evolving Solar Wind Streams and Shocks Beyond 1 AU. In *Study of Traveling Interplanetary Phenomena*, eds. M. A. Shea, D. F. Smart, S. T. Wu (Dordrecht: D. Reidel Pub. Co.) p. 227.
- Smith, E. J. 1989. Interplanetary magnetic field over two solar cycles and out to 20 AU. *Adv. Space Res.*, 9:159-169.
- Smith, **E.J.** 1985. Interplanetary shock phenomena beyond 1 AU. In *Collisionless Shocks in the Heliosphere: Reviews of Current Research*, 35, eds. **B.T.** Tsurutani and Robert G. Stone (Washington, D.C.: American Geophysical Union) p. 69.
- Snyder, C. W., and **Neugebauer**, M. 1964. Interplanetary solar wind measurements by Mariner 2. *Space Res.* 4:89-113.
- Suess, S. T., and **Nerney**, S. F. 1975. The global solar wind and predictions for Pioneers 10 and 11. *Geophys. Res. Lett.*, 2:75.
- Suess, S. T., and Richter, A. K., Winge, C. R. and **Nerney**, S. F. 1977. South Polar Coronal Hole - A Mathematical Simulation. *Astrophys. J.*, 217:296-305.
- Suess, S. T., Thomas, B. T. and **Nerney**, S. F. 1985. Theoretical Interpretation of the Observed Interplanetary Magnetic Field Radial Variation in the Outer Solar System. *J. Geophys. Res.*, 90:4378.
- Svalgaard, L. and Wilcox, J, **M.** 1974. The spiral interplanetary magnetic field: A polarity and sunspot cycle variation. *Science* 186:51.

Thomas, B. T., and Smith, E. J. 1980. The Parker Spiral Configuration of the Interplanetary Magnetic Field Between 1 AU and 8.5 AU. *J. Geophys. Res.*, 85:6861.

Wang, Y.-M. 1995. Latitude and solar cycle dependence of radial IMF intensity. *Space Sci. Rev.*, 72:193-196.

Wenzel, K.-P., Marsden, R. G., Page, D. E. and Smith, E. J. 1992. The Ulysses mission. *Astron. Astrophys. Suppl. Ser.*, 92:207.

Winterhalter, D., Smith, E. J., Wolfe, J. H., and Slavin, J. A. 1990. Spatial gradients in the heliospheric magnetic field: Pioneer 11 observations between 1 AU and 24 AU, and over solar cycle 21. *J. Geophys. Res.*, 95:1.

Zhao, X-P. and Hundhausen, A. J. 1981. Organization of solar wind plasma properties in a tilted, heliomagnetic coordinate system. *J. Geophys. Res.*, 86:5423.

Zhao, X-P. and Hoeksema, J.T. 1995. Modeling the Out-Of-Ecliptic Interplanetary Magnetic Field in the Declining Phase of Sunspot Cycle 22. *Space Sci. Rev.*, 72:189-192.

Zirker, J.B. 1977. Coronal holes -An overview, In: *Coronal Holes and High Speed Wind Streams*, ed. J.B. Zirker (Boulder: Colorado Associated University Press), pp. 1-26.

FIGURE CAPTIONS

Figure 1. The Parker Spiral

Spiraling magnetic field lines are shown emanating from the Sun and being carried out to 1AU (the dashed circle). The spiral angle between the radial direction and the field is larger than the more typical angle of 45° because a relatively low velocity (300 km/sec) was assumed in deriving the figure. The radial lines represent the solar wind velocity. Arrows have been added

showing the field polarity and the corresponding pluses and minuses give rise to the so-called magnetic sectors (two in this instance). A pair of oppositely-directed field lines coincide with the sector boundaries (S/B).

Figure 2. Latitudinal angle of the magnetic field

The instantaneous latitudes of \vec{B} (called theta here) relative to the **radial** direction have been assembled to form this histogram. Pioneer 10 and 11 data acquired between 1 and **8.5AU** are represented. The prediction of the Parker model that there would be no non-zero average latitude angle or, equivalently, no average north-south component is borne out by the observations.

Figure 3. Longitude angle of the magnetic field

In order to test the prediction that the longitude angle (phi) coincides on the average with the Archimedes spiral, the observed field longitude angles were transformed into a coordinate system with one axis along the spiral direction. The Pioneer spacecraft were traveling from 1 to **8.5AU** during the interval represented by these data and this choice of coordinates automatically took into account the radial dependence of phi. The two peaks correspond to a spiral angle of 45° at 1AU and shows the presence of the two sector polarities.

Figure 4. The sector structure at **1AU** and in the outer **heliosphere**

The column on the left shows the **sector** structure each solar rotation as determined from **IMP** and/or **ISEE-3** data at 1 AU. In the right column are the **corresponding** sectors observed by Pioneer 11 as it progressed from 1 to **12AU**. The 9-year interval includes solar minimum (1976), maximum (1979) and the descent toward the next minimum. There is substantial agreement in the sector structure in spite of the increasing radial distance of Pioneer 11.

Figure 5. Field longitude angle observed at 35AU

The field longitude angle is shown based on hourly **averages** acquired by Pioneer 11 in 1991 near 35 AU. The spiral angle and the inward and outward sectors (approximately* 90° here corresponding to the wrapping-up of the field with distance) are clearly identified. There is a relative absence of other directions (note the depth of the minima near 0° and 180°) such as might be anticipated if the current sheet was becoming “tattered” or tending to disappear.

Figure 6. Schematic of the solar wind magnetic field **lines** near the Sun

The closed fields (loops) begin and end on the Sun. The open field lines have only one end on the Sun, the other “end” being carried off by the solar wind. The dotted surface is the **heliospheric current** sheet. It is shown as warped because the equivalent magnetic symmetry axis, M , does not coincide with the Sun’s rotation axis.

Figure 7. Variation of solar wind density and velocity with latitude above and below the **heliospheric** current sheet

The **heliomagnetic** latitude is the spacecraft latitude relative to the magnetic equator or the current sheet rather than to the Sun’s rotation equator, The. speed is low and the density is high near the current sheet.

Figure 8. Magnetic fields at the photosphere and on the solar wind **source** surface

The upper figure is a synoptic representation of the **photospheric** field strength and polarity along the line-of-sight to an earth-based **magnetograph**. A **single** solar Barrington rotation (1 848) is shown. The lower figure shows the corresponding smoother contours after the observed fields are extrapolated to a spherical surface at 2.5AU and subjected to a boundary condition that the field be radial there.

Figure 9. Solar cycle variations in the Sun’s magnetic **field**

Inferred properties of the solar field **are** shown during the recent sunspot cycle (1976-1991). The upper curve of the polar field strength shows polarity reversals in 1979-1980 and 1990. The dark line is the smoothed average of the annual variations in the north (light solid line) and south (dashed line) polar fields. The middle panel shows the dipole angle which systematically rotated from being aligned with the rotation axis (90°) during the 1976 minimum to being equatorial (0°) at the maxima in 1979 and 1990. The bottom curve shows the maximum current sheet inclination (tilt angle) on the source surface and follows the middle panel.

Figure 10. Pioneer 11 observations of the disappearance of the sector structure at 15° latitude Data from two successive minima **in** 1976 and 1986 are shown. In the left figure, fields corresponding to positive polarity or outward fields are seen to be continuously present at

northern latitudes because the current sheet inclination is less than the latitude of the spacecraft. In the right figure, ten years later, the opposite situation **prevails**. Negative polarity or **inward**-directed field are seen continuously, again corresponding with the fields in the Sun's northern hemisphere.

Figure 11. Correlation between the differences in magnetic polarity at two spacecraft and their differences in latitude

The observations were obtained simultaneously at **ISEE-3** and Pioneer 11 which were located at significantly different heliographic latitudes as shown. The variations are caused by the annual excursion of **ISEE-3** as it orbits the Sun in the ecliptic plane at an inclination of $7\frac{1}{4}^{\circ}$ to the rotation axis. At each spacecraft, the fraction of each solar rotation that a positive polarity was observed, $P(+)$, was found and the differences are shown, During 1976, when Pioneer 11 was above **ISEE-3**, an excess positive polarity was seen. The phase between the two curves reversed in 1979-1980 when the Sun's polar caps reversed polarity.

Figure 12. Schematic representation of corotating interaction regions

Magnetic fields and solar wind streamlines are shown in the upper figure in a coordinate system rotating with the Sun. This schematic and the variations in the field and solar wind parameters shown in the lower half-figure are appropriate to conditions near 1 AU. At larger distances the edges of the **interaction/compression** region steepen into shocks.

Figure 13. A pair of forward and reverse shocks bounding a corotating interaction region (**CIR**) The **field** magnitude and speed are shown at 4.3AU as observed **by** Pioneer 10 over an interval of several days. The abrupt increase in B and V corresponds to a forward shock as indicated in the diagram at the bottom. The increase in V with a simultaneous decrease in B coincides with a reverse shock.

Figure 14. Magnetic field variations at large distance **compared** with those at 1 AU

The upper panel contains daily averages of B at Pioneer 11 which was located at 16AU. A single large increase tends to be seen each solar rotation. The lower panel contains comparable observations made at 1 AU by the International Cometary Explorer/**ICE** (formerly **ISEE-3**).

Many increases in B are seen each rotation which must have merged by the time they reached 16AU.

Figure 15. A comparison of field magnitudes at 1 AU and in the outer heliosphere

The upper curve (open symbols) consists of annual averages of B at 1 AU as measured by several spacecraft between 1973 and 1992. The lower curve (solid dots) are annual averages of the field magnitude measured at Pioneer 11 but extrapolated back to 1 AU using the Parker solar wind model. During this 20-year interval, Pioneer traveled out to beyond 30AU. The comparison shows the solar cycle variation in B at both locations but with lower fields at the larger distances than would be expected on the basis of the model. The difference, called the magnetic flux deficit, has generated a considerable controversy in the recent scientific literature.

Figure 16. Example of a “magnetic cloud”

The “cloud” shown here is based on **Helios** 1 data. The **magnitude** and two angles (latitude, longitude) of the magnetic field and the solar wind velocity, density and temperature are shown. “Magnetic clouds” are a subset of CMES identified solely by their magnetic properties of which this is a representative example.

Figure 17. Schematic of the CME as a flux rope

The possible magnetic topology of a CME is shown. Both examples show the CME as a magnetic “tongue” or “bottle” with the field lines attached to the Sun (closed). In the lower half-figure, the field lines form a helix which could correspond to a force-free field configuration.

Figure 18. Simulation of a series of CMES as they expand into the outer heliosphere

The expansions of a series of six successive CMES from the same solar longitude are shown between the Sun and 15AU. The **dark** regions are magnetic fields that are compressed by the on-coming CME. The lighter regions are expansion regions within the CME proper. The combined effect of the several CMES could be to form a barrier (a global merged interaction region) that opposes the entry of cosmic rays.

Figure 19. Magnetic field just inside the heliopause

In this cylindrical coordinate system, the streamlines are shown as originating at the stagnation point between the **heliopause** and the interstellar plasma wind. They then turn and flow parallel to the **heliopause** along the inside. Representative magnetic field lines are also shown. They are parallel to the flow along the equator (the plane perpendicular to the solar rotation axis) but perpendicular to the flow and significantly greater in magnitude over the solar poles.

Figure 20. The **heliospheric** magnetic field in three dimensions

Open magnetic field lines originating at three latitudes **are** shown in the form of **helices**. In the equator, the field lines are tightly wound, take the form of a coiled spring and are transverse to the flow. At higher latitudes the field lines lie on the surface of a cone and are less tightly wound, especially near the Sun's pole where they are nearly **radial** and parallel to the solar wind (represented by the arrows).

Figure 21. Profile of the Ulysses mission

Ulysses was launched in October, 1990 into a low inclination elliptical orbit with aphelion near the orbit of Jupiter. The spacecraft encountered Jupiter in February, 1992 and was gravitationally redirected into a high inclination orbit. The resulting trajectory is a large ellipse inclined 80° to the solar equator with a perihelion of 1.1 AU, an aphelion of 5.2 AU and a period of 6.3 years. It reaches maximum latitudes in September 1994 (south) and August 1995 (north).

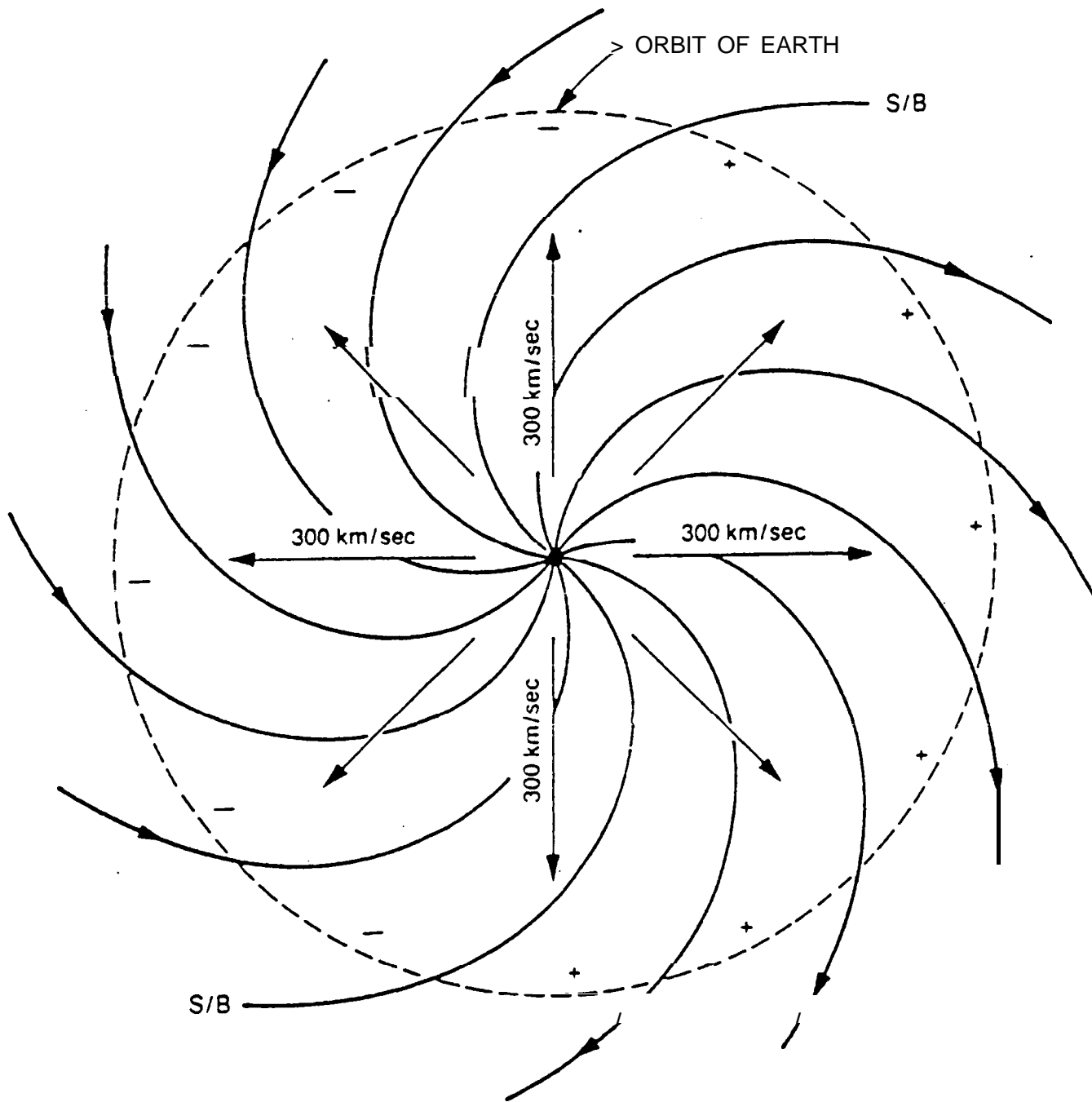
Figure 22. The radial magnetic field at Ulysses and in the ecliptic

Averages of B_{PR}^2 at Ulysses over 5° increments in latitude. (top) are shown as a function of time (bottom). Also shown **are** averages of B_R over the same time intervals measured by the IMP-8 spacecraft inside negative magnetic sectors. The correspondence of the time variations at both locations and the absence of a significant latitude gradient are evident,

Figure 23. The spiral angle observed by Ulysses at high latitudes

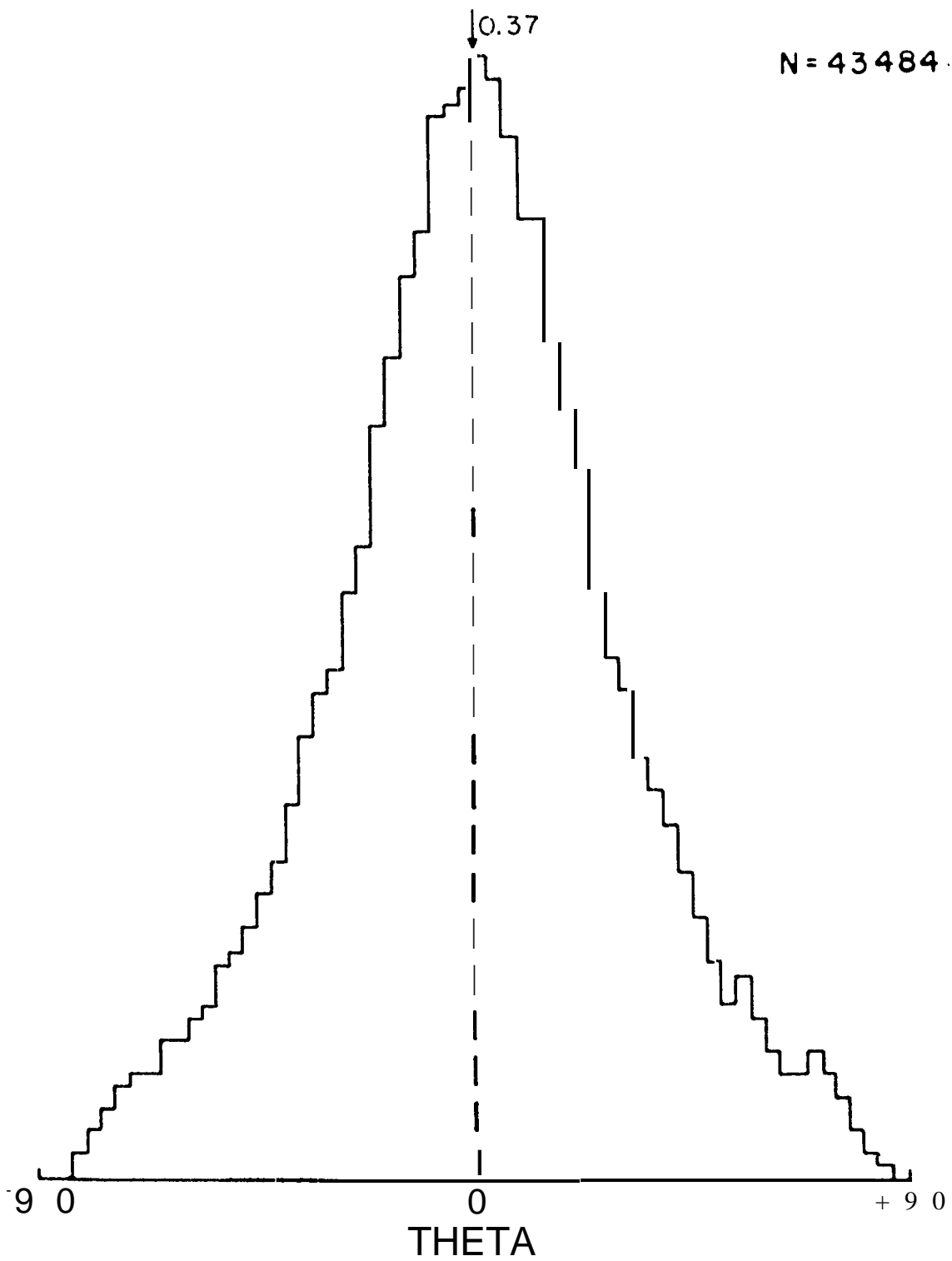
Hourly averages of Φ_B obtained above 60° latitude were used to prepare this histogram. The value of the Parker spiral, obtained from the hourly average of the solar wind speed, was subtracted from Φ_B so that the histogram represents deviations from the Parker spiral. The most probable value is negative implying the field is too tightly wound. However, because of the

asymmetry in the distribution, the overall average is positive corresponding to the field being underwound,



2

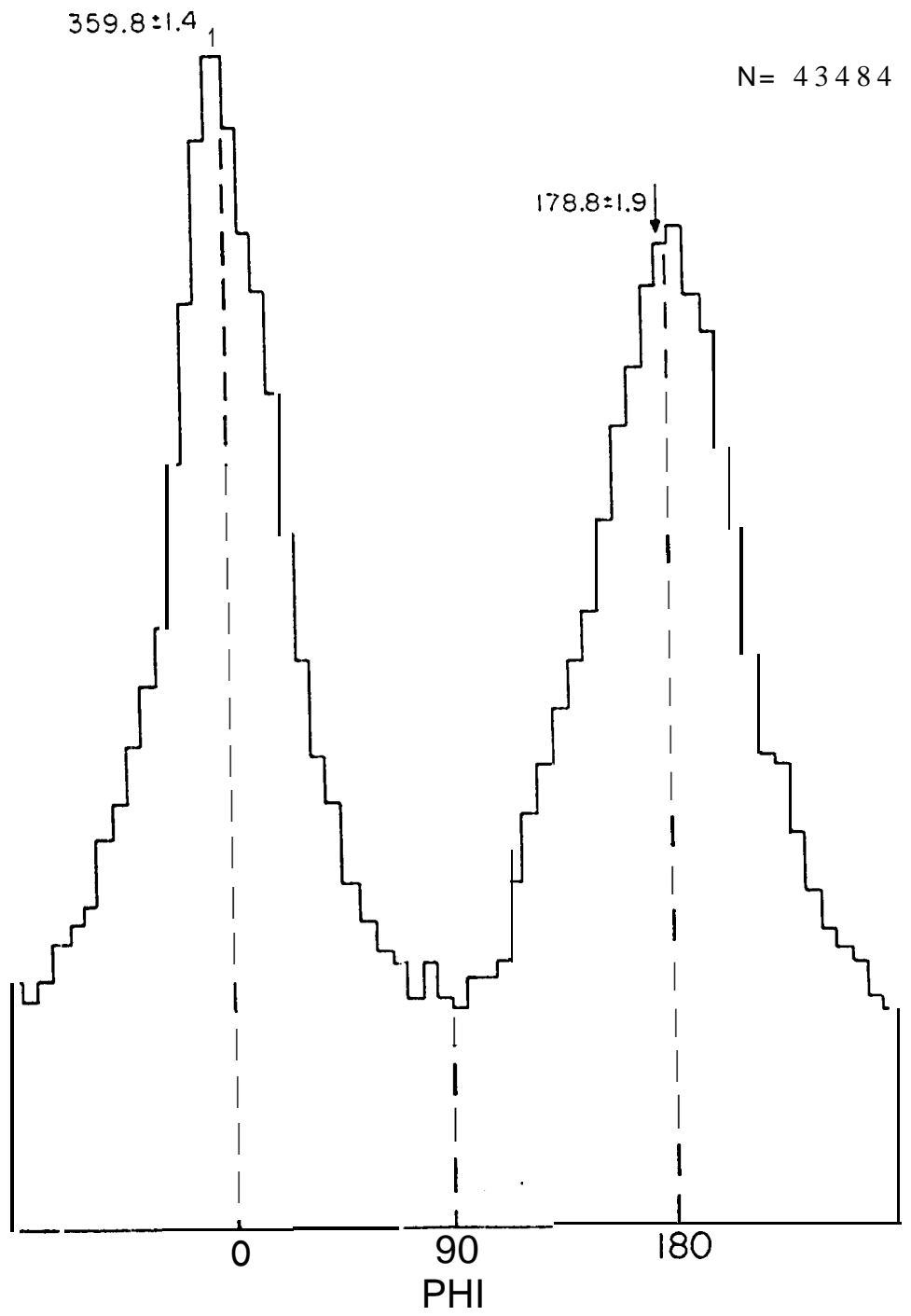
PIONEER 10 AND 1 ALL DATA



2

7

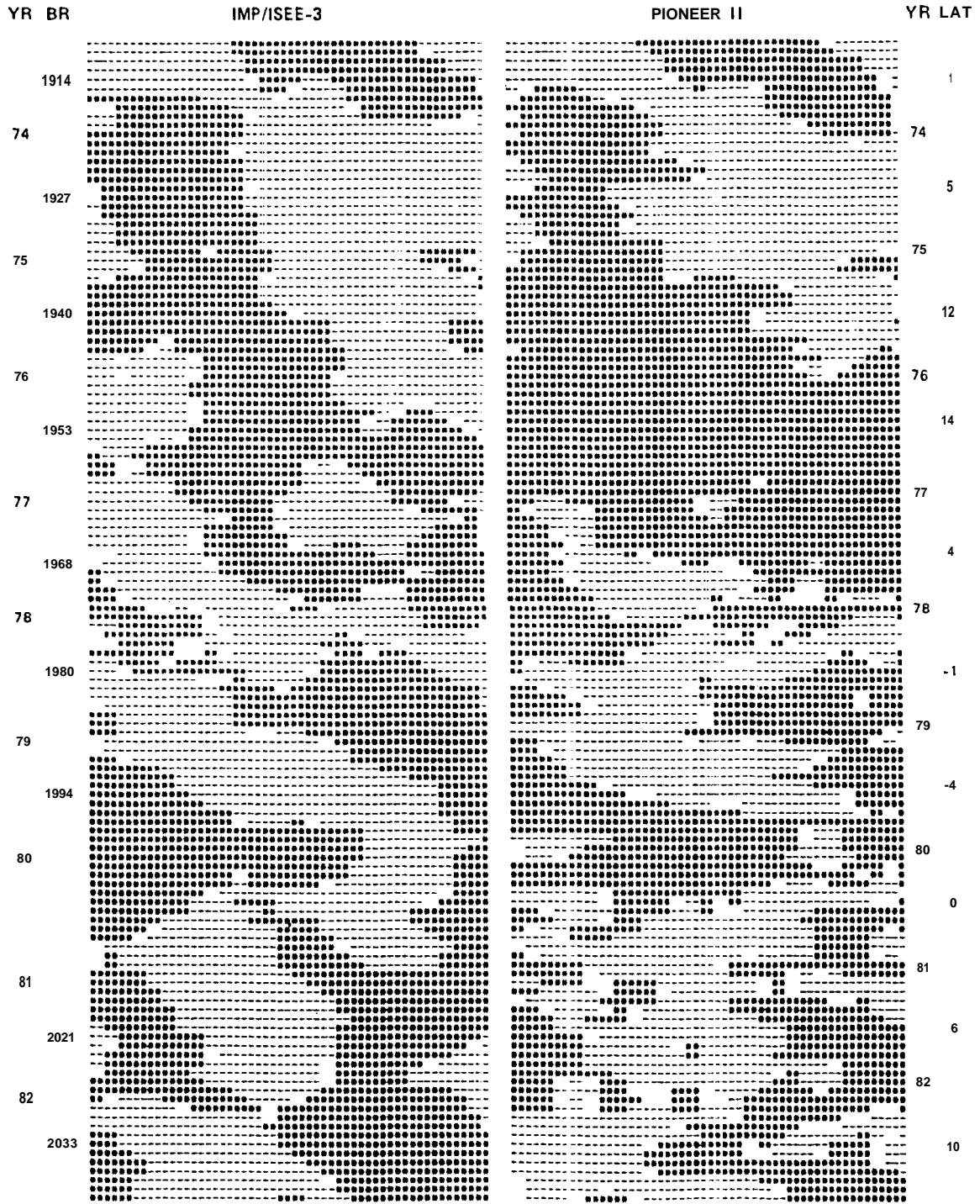
PIONEER 10 AND II ALL DATA



3
#

8

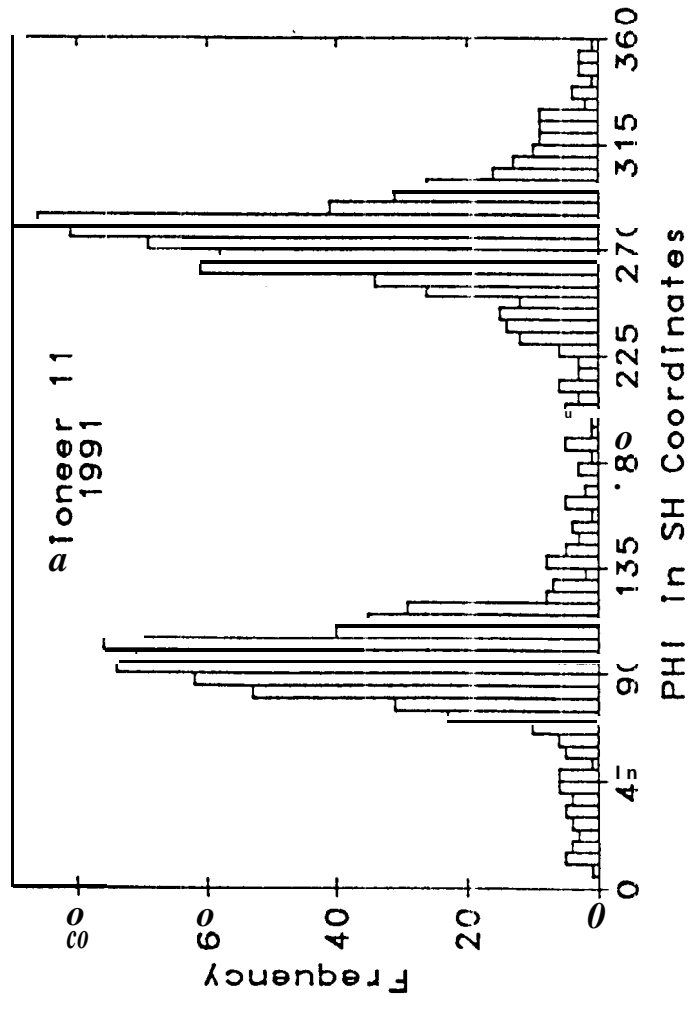
INTERPLANETARY SECTOR STRUCTURE

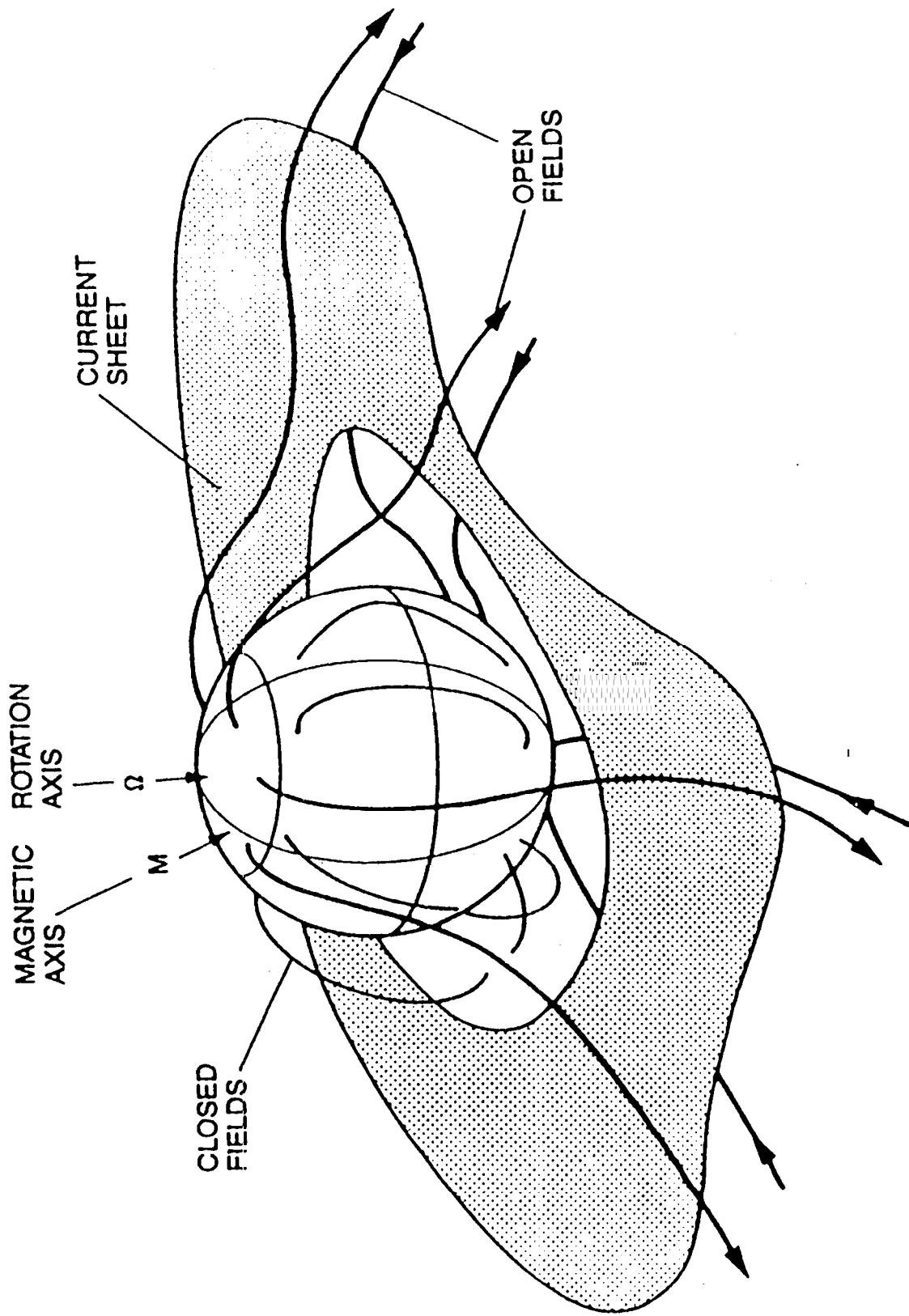


DAY OF BARTELS ROTATION

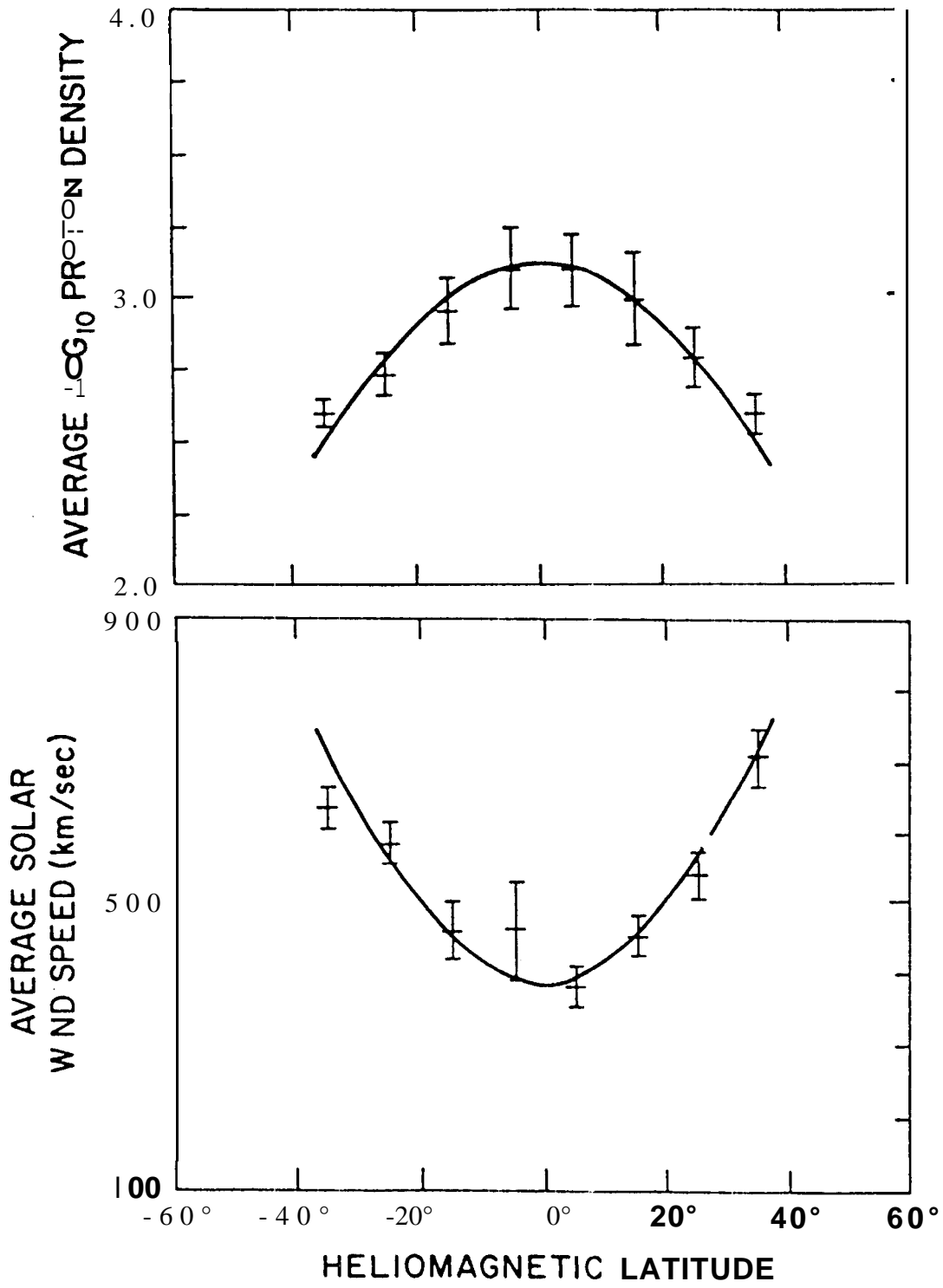
4

MB





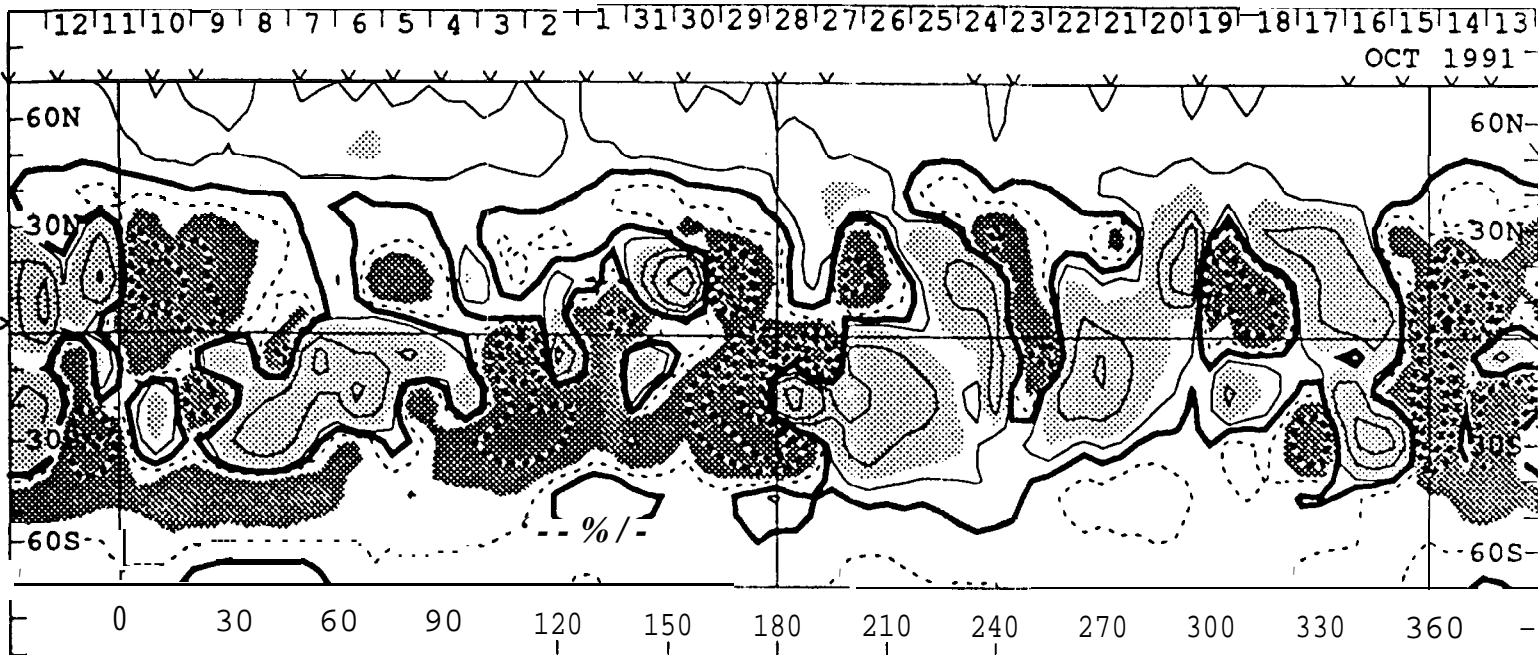
6



7

Photospheric Magnetic Field

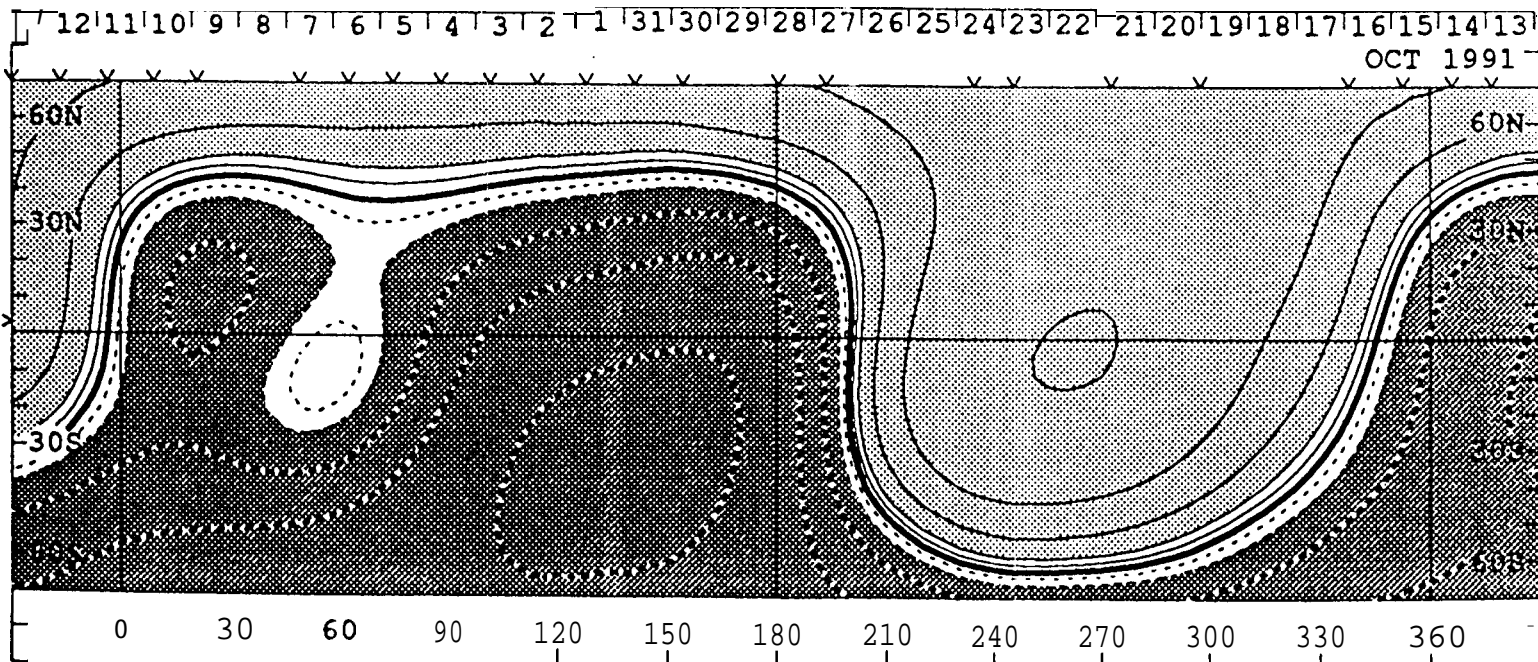
0, +100, 500, 1000, 2000 MicroTesla



1848

Source Surface Field

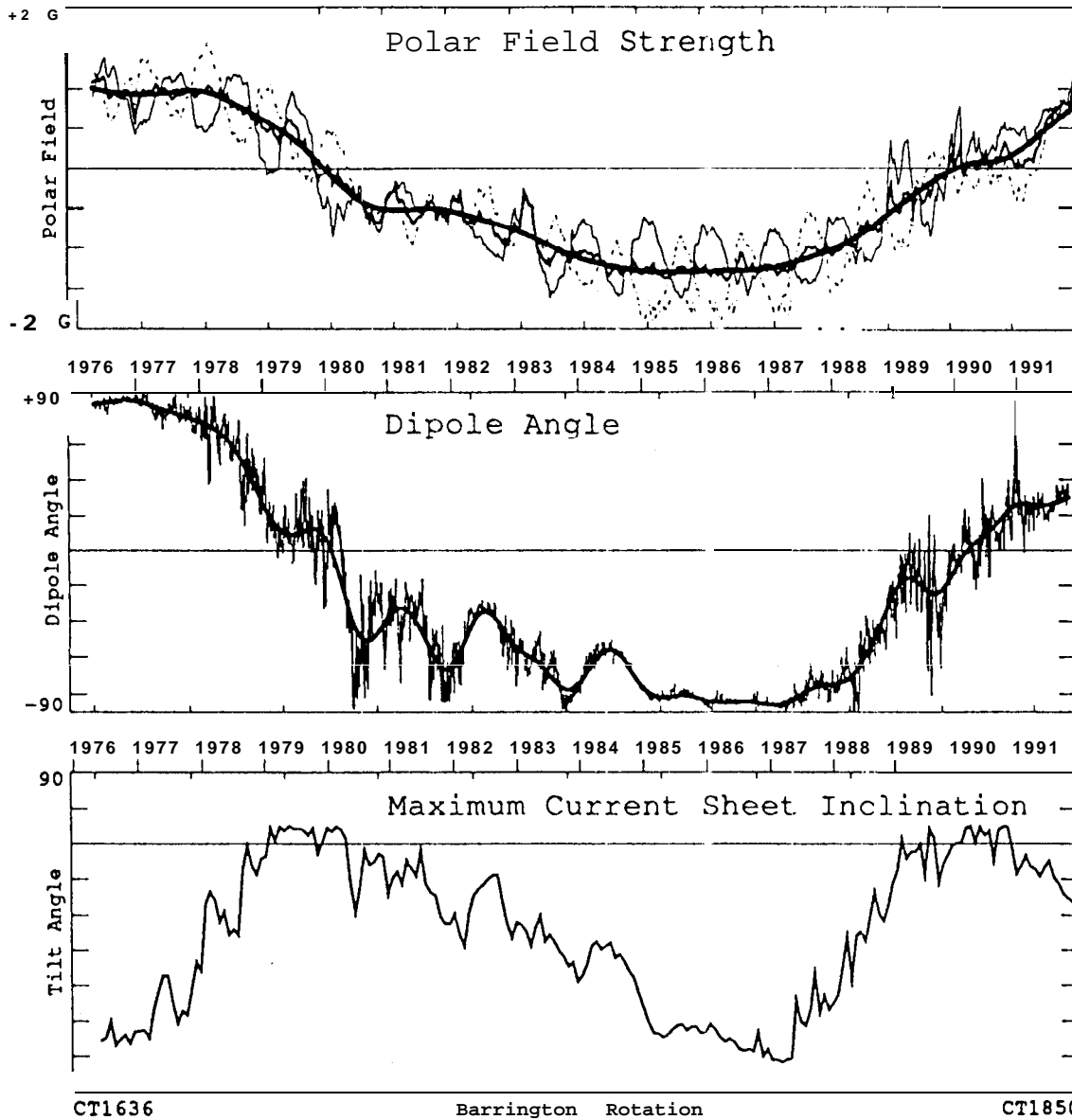
0, +1, 2, 5, 10, 20 MicroTesla



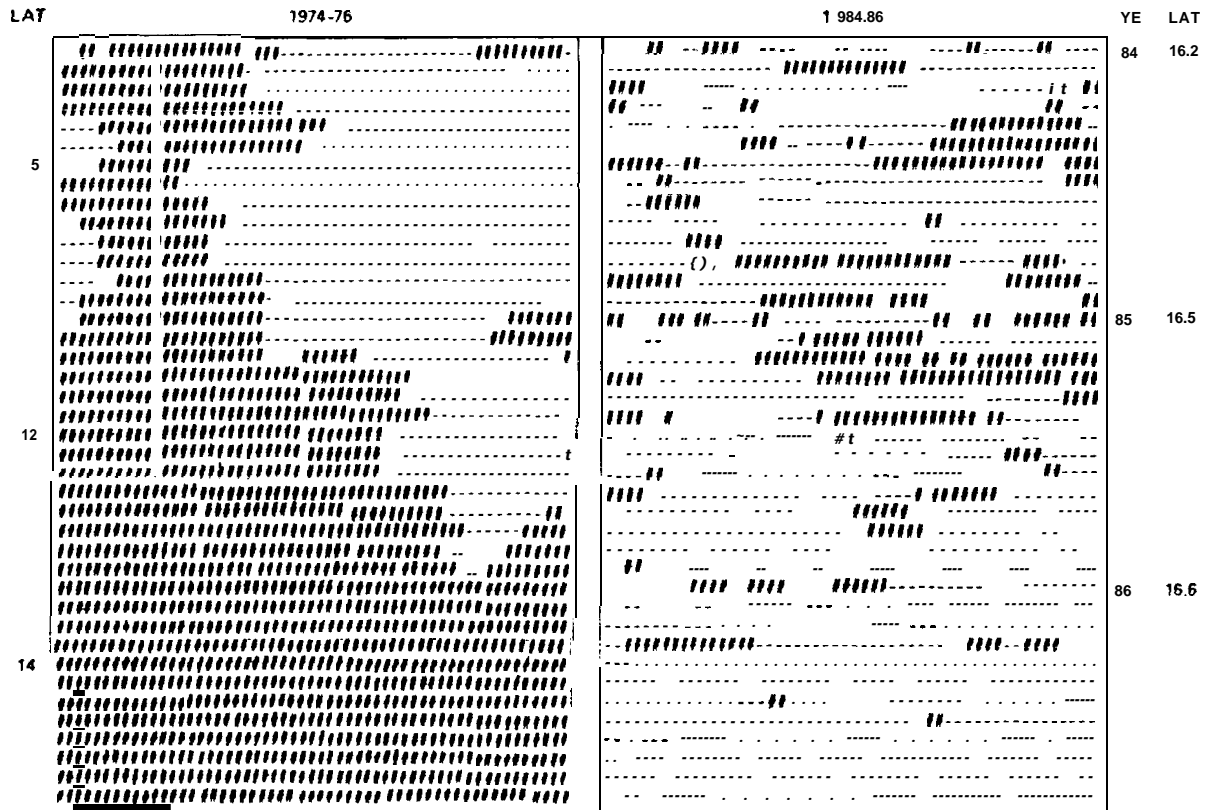
1848

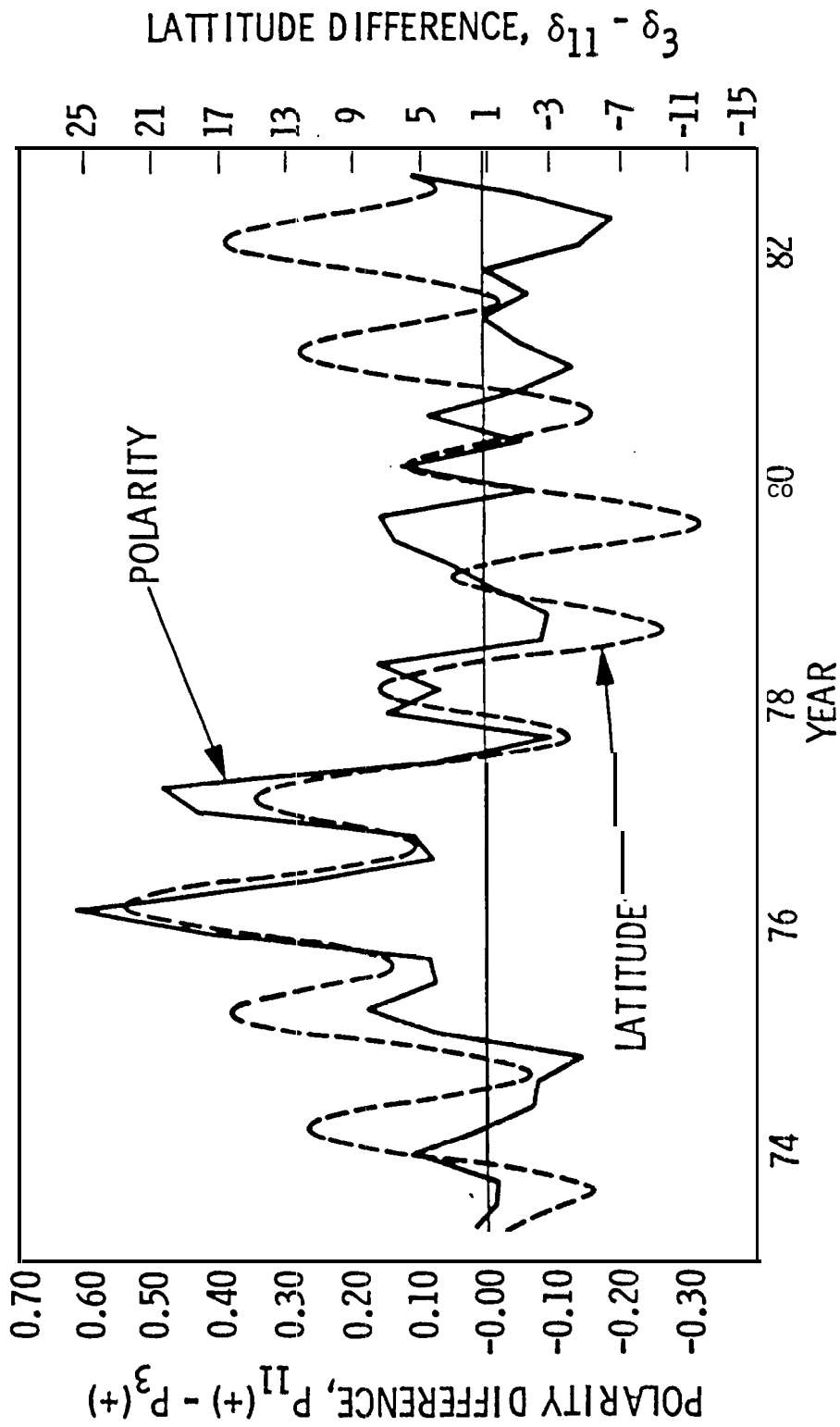
b.

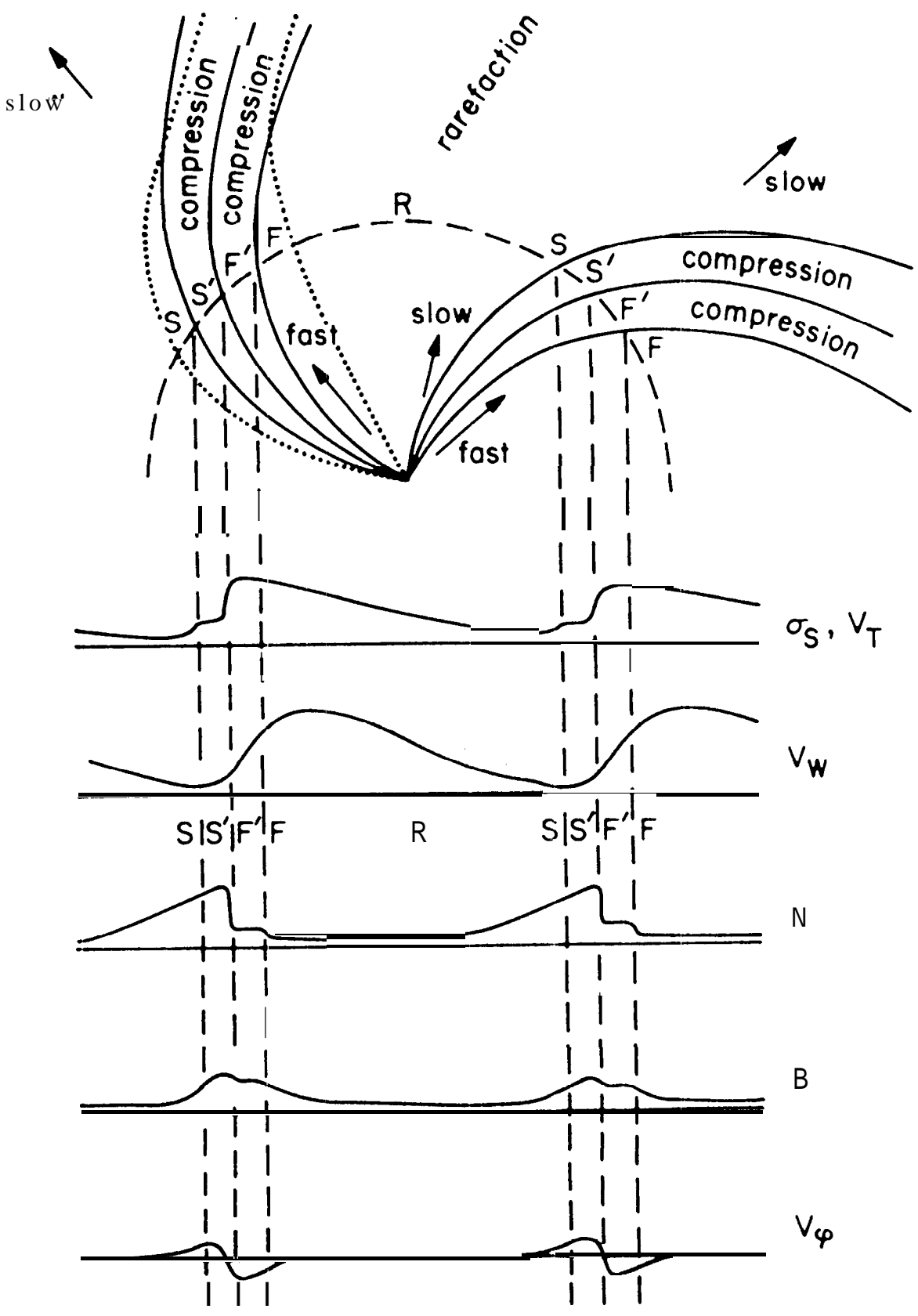
Solar Cycle Variations

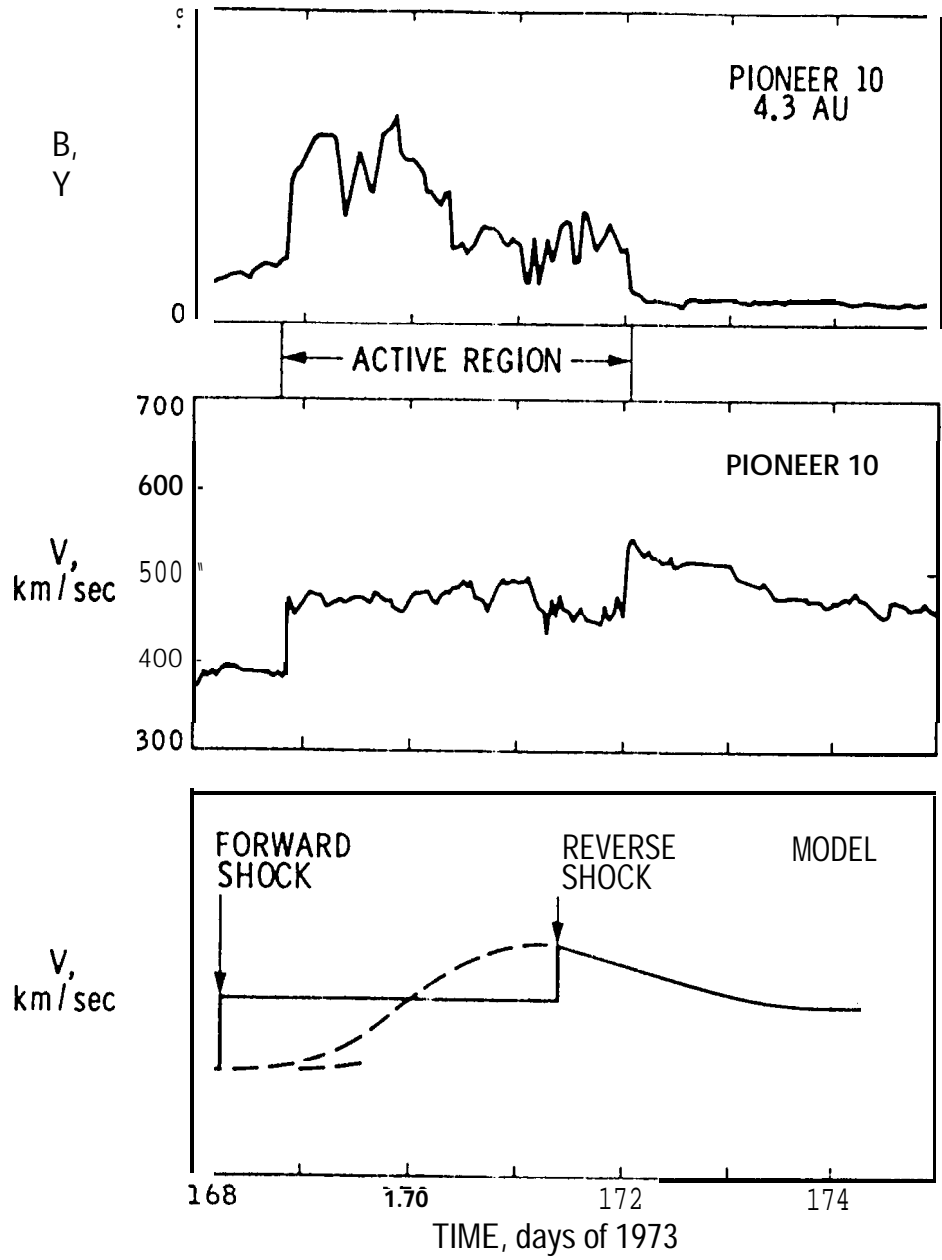


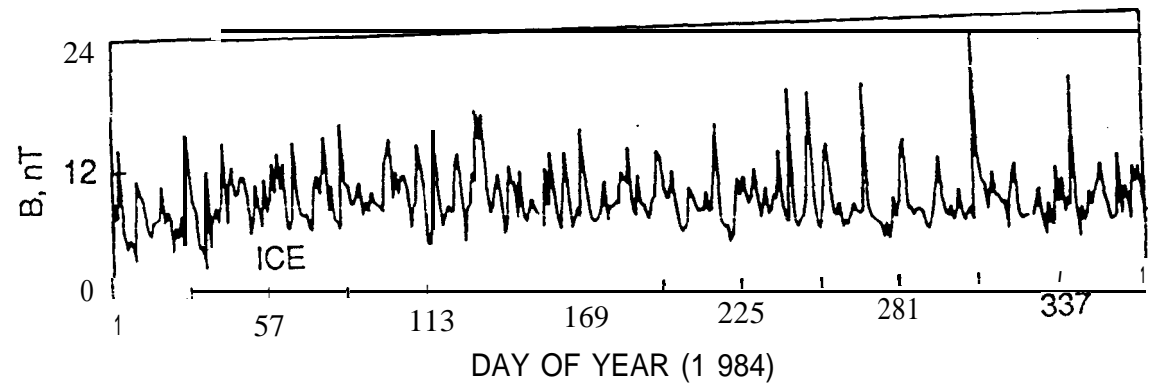
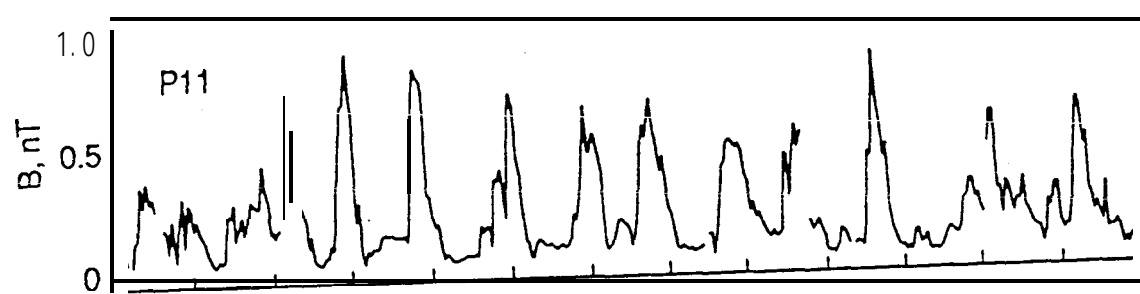
SECTOR STRUCTURE - PIONEER 11







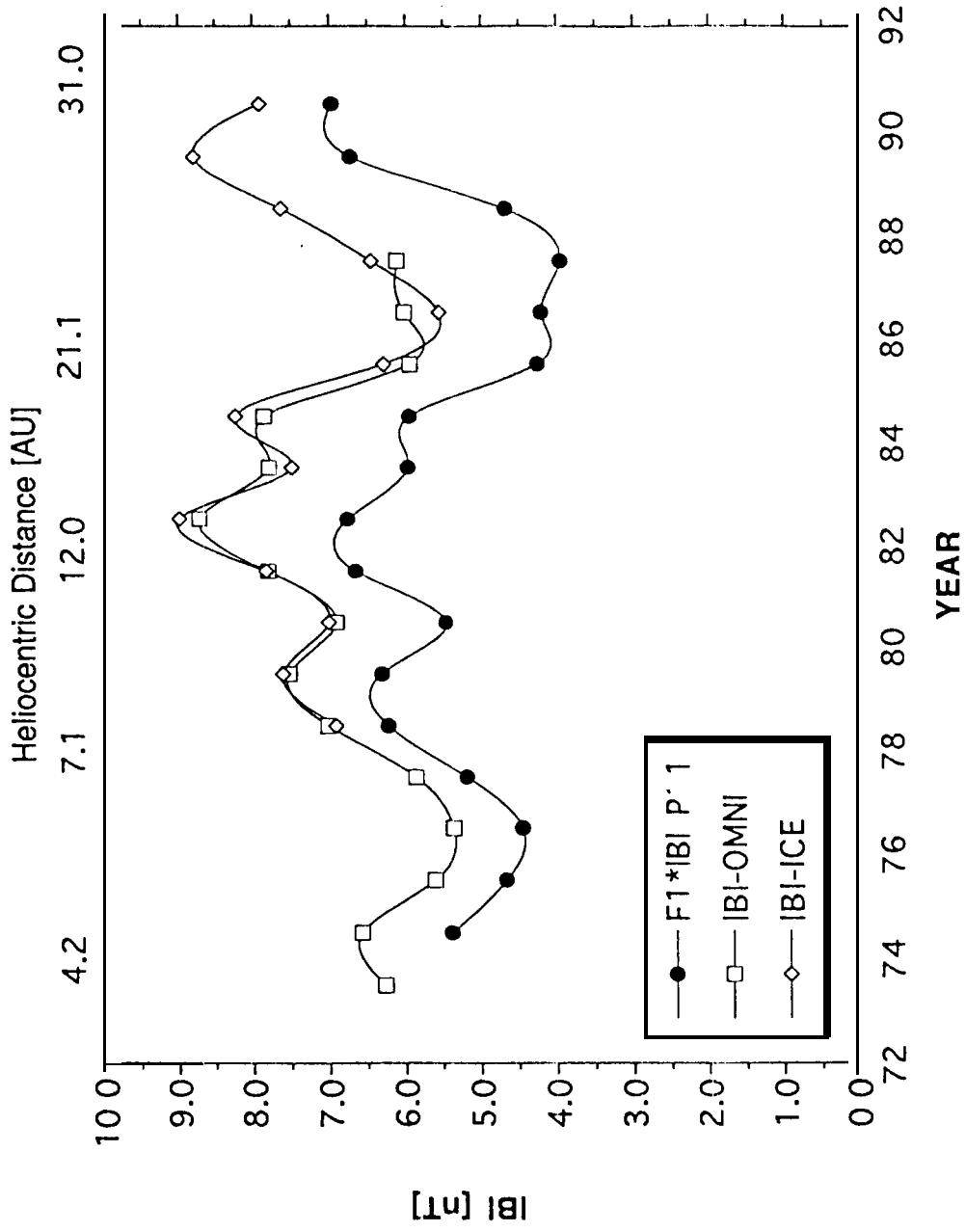




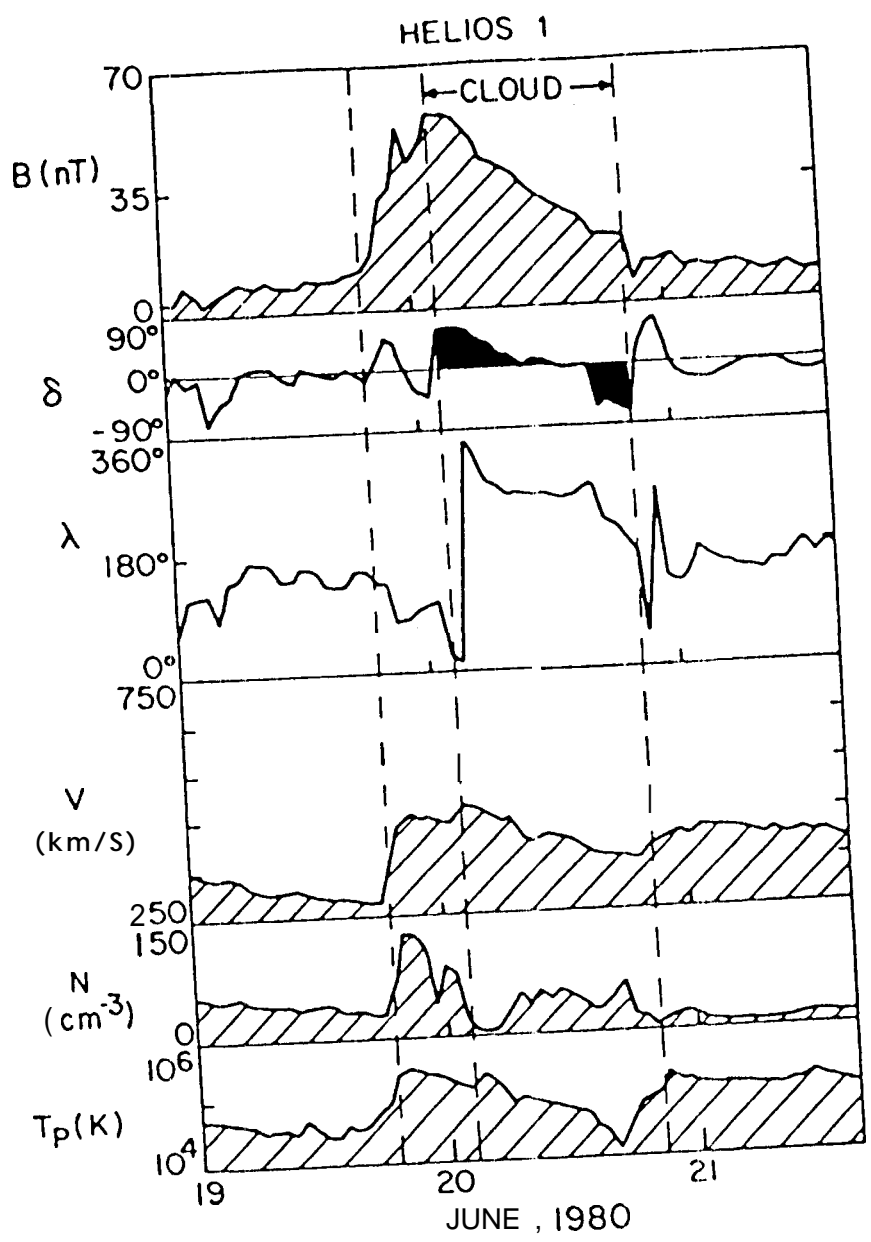
14

14

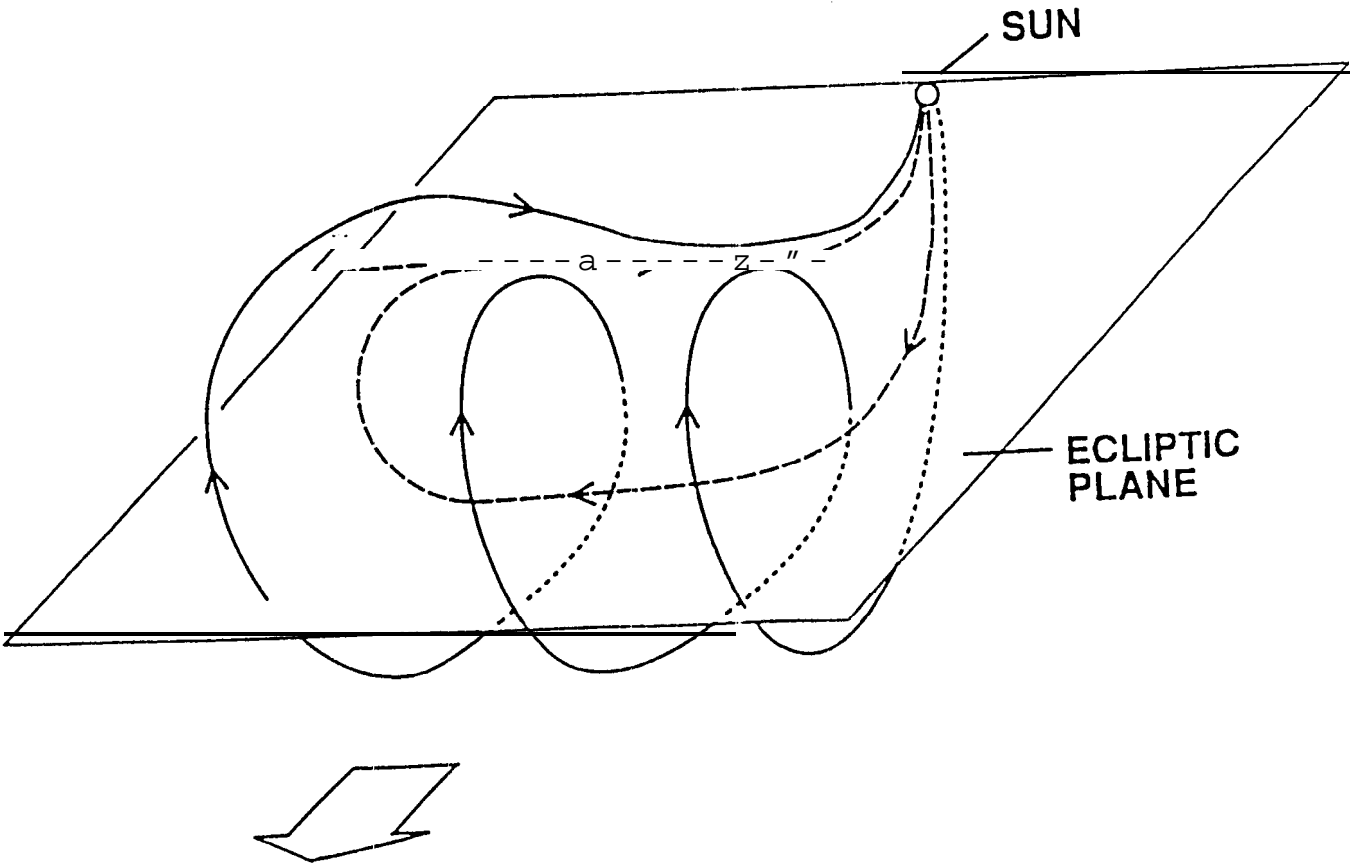
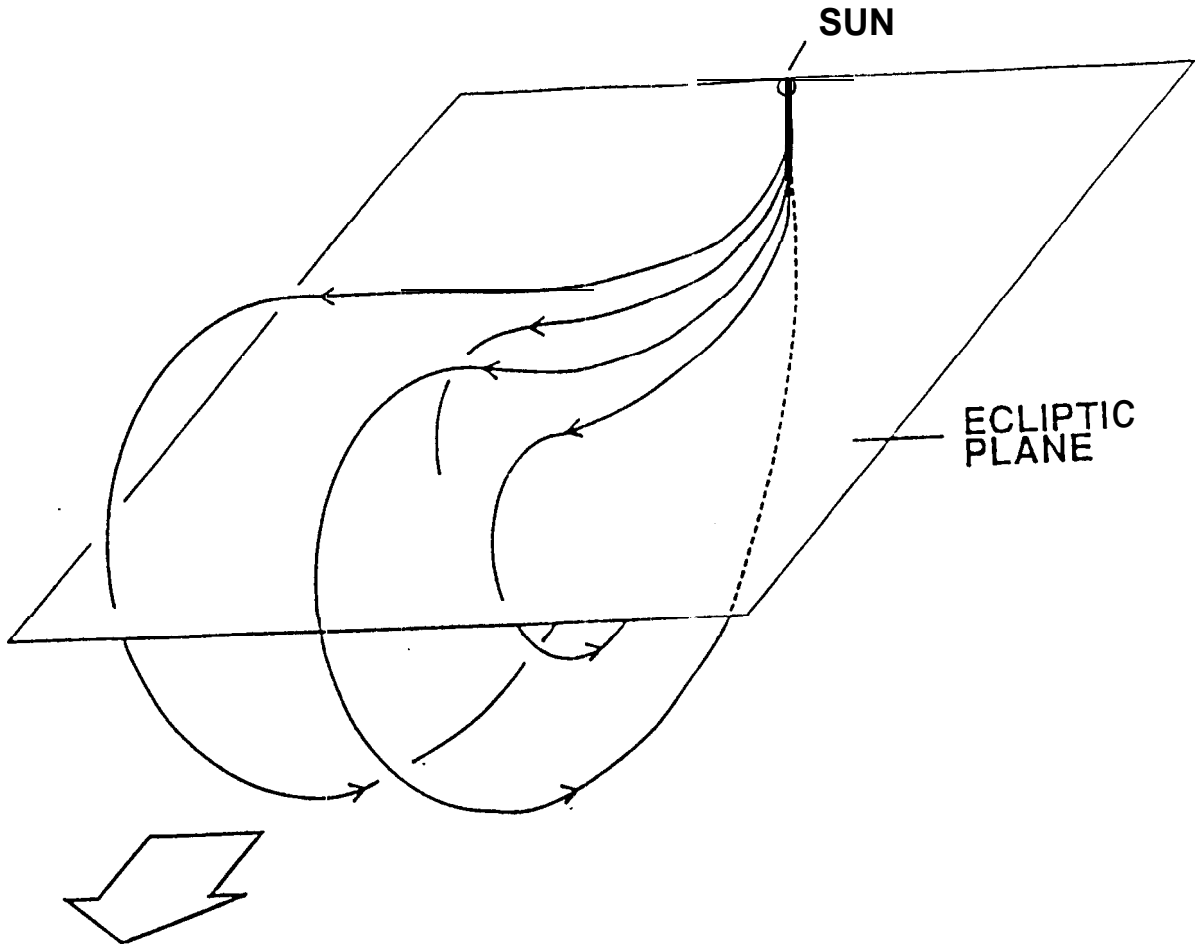
PIONEER 11 MAGNETOMETER



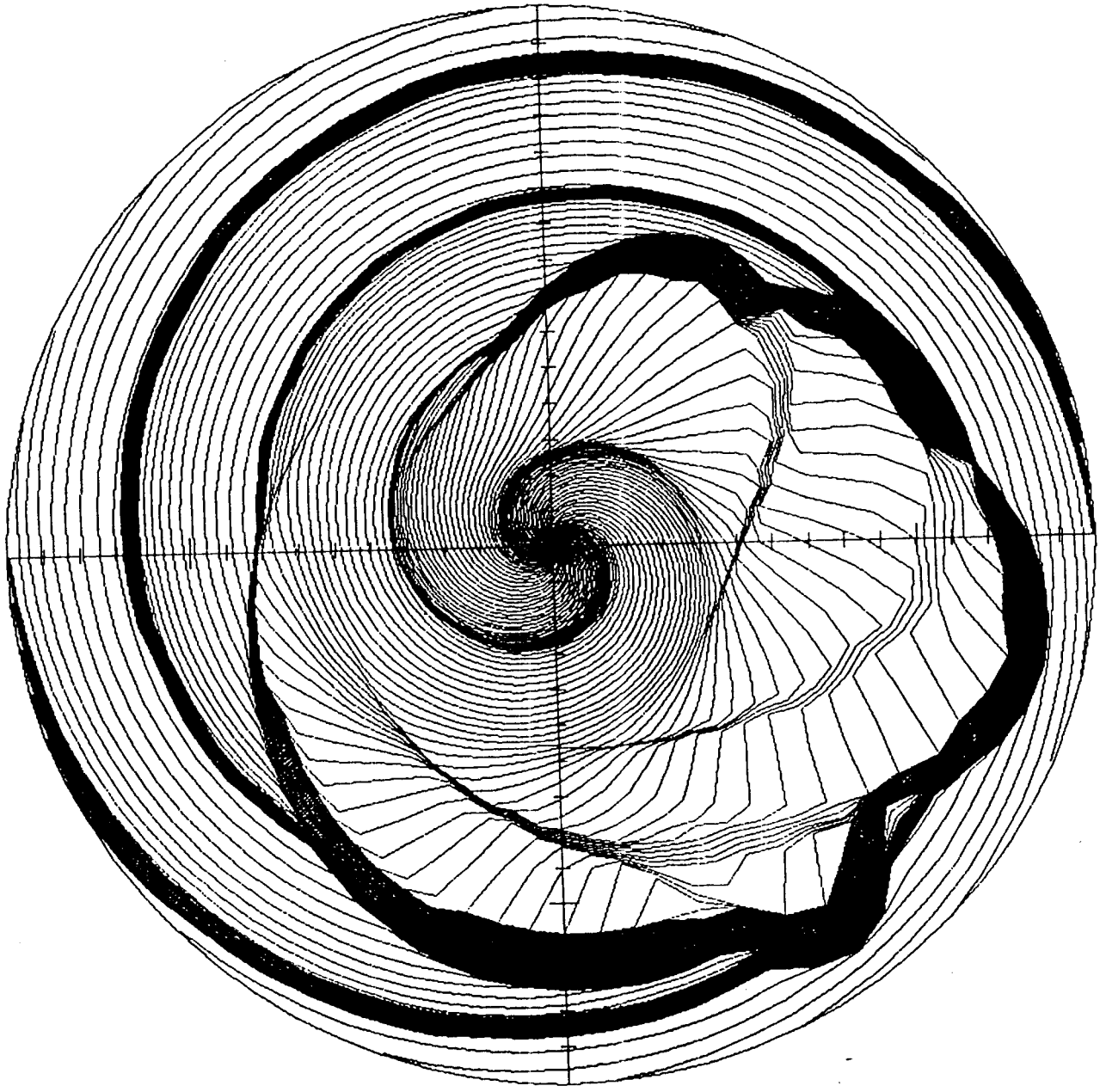
91



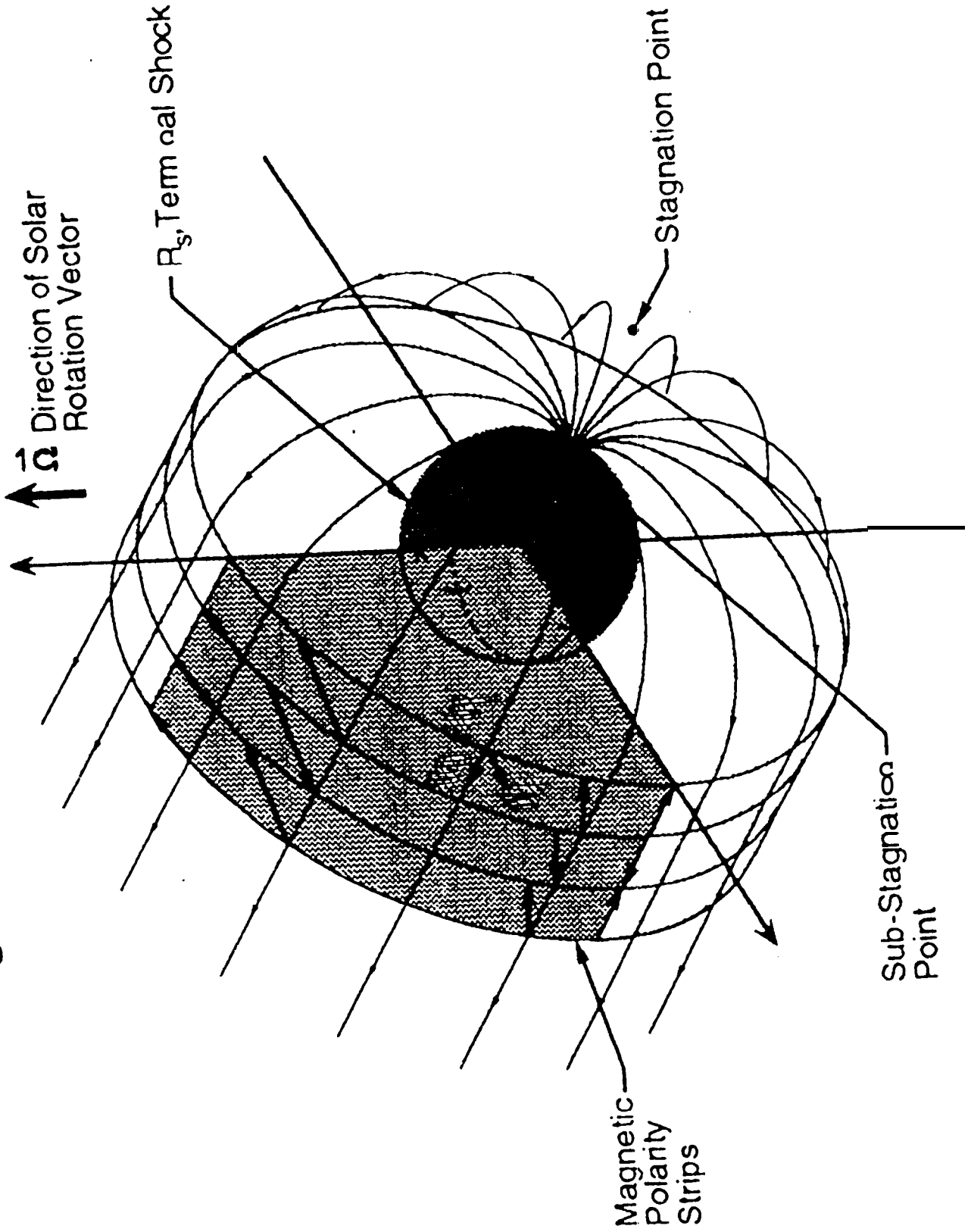
61 . . .

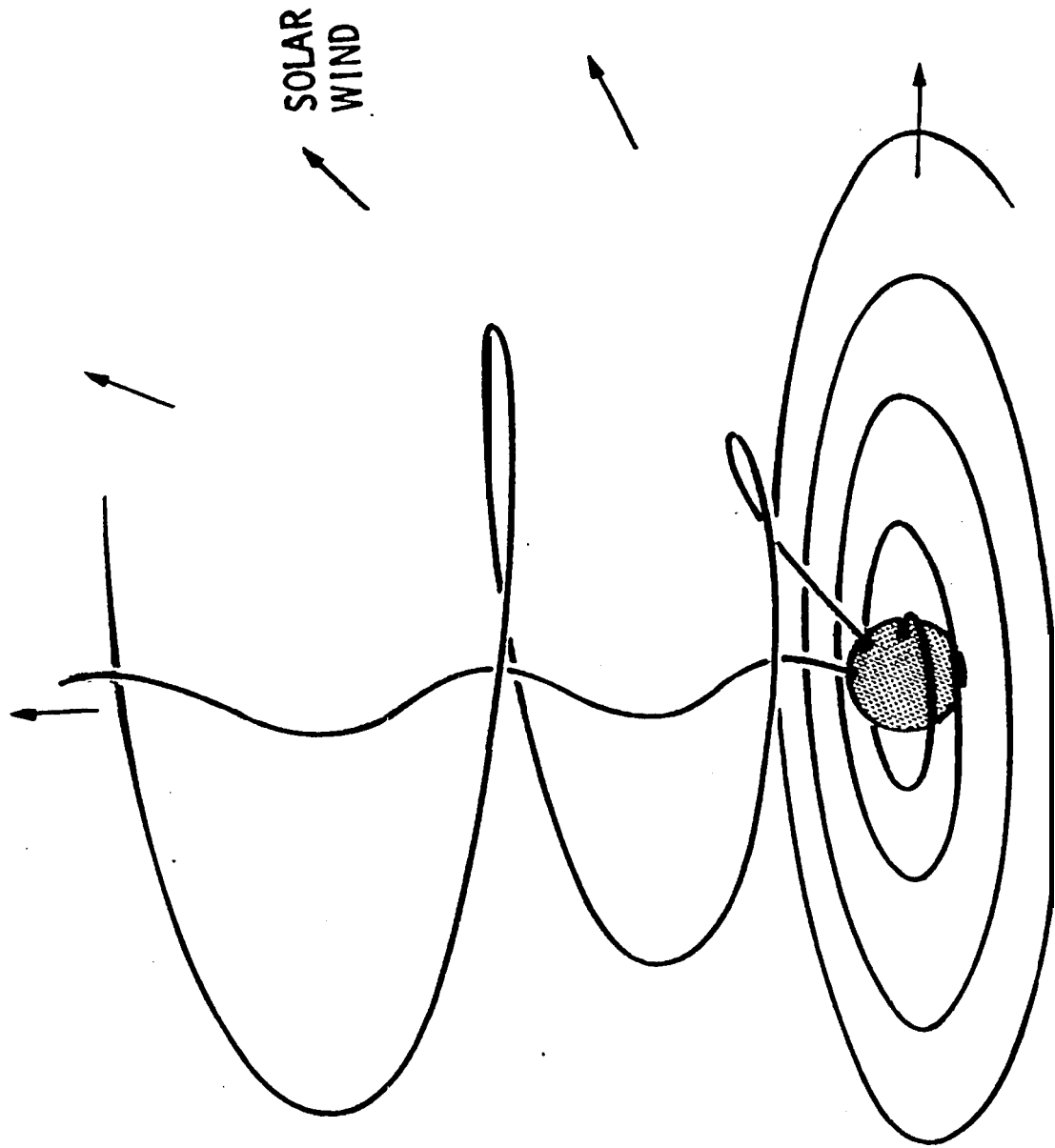


81 .



Magnetic Field $\mathbf{0} \times \text{eliopause Surface}$





ULYSSES MISSION PROFILE

